

Article

Implementation of Atomically Thick Graphene and Its Derivatives in Electromagnetic Absorbers

Jing Tian ¹, Hongyu Shi ², Haoquan Hu ¹, Bo Chen ¹, Yongfang Bao ¹ and Pu Tang ^{1,*}

¹ School of Electronic Science and Engineering, University of Electronic Science and Technology of China, Chengdu 611731, China; j.tian@uestc.edu.cn (J.T.); huhq@uestc.edu.cn (H.H.); chenbo@uestc.edu.cn (B.C.); yfbao@uestc.edu.cn (Y.B.)

² School of Electronic and Information Engineering, Xi'an Jiaotong University, Xi'an 710049, China; honyo.shi1987@gmail.com

* Correspondence: putang@uestc.edu.cn

Received: 29 December 2018; Accepted: 19 January 2019; Published: 23 January 2019



Abstract: To reduce the radar cross section at microwave frequencies, it is necessary to implement electromagnetic (EM) absorbing devices/materials to decrease the strength of reflected waves. In addition, EM absorbers also find their applications at higher spectrum such as THz and optical frequencies. As an atomic-thick two-dimensional (2D) material, graphene has been widely used in the development of EM devices. The conductivity of graphene can be electrostatically or chemically tuned from microwave to optical light frequencies, enabling the design of reconfigurable graphene EM absorbers. Meanwhile, the derivatives of graphene such as reduced graphene oxide (rGO) also demonstrate excellent wave absorbing properties when mixed with other materials. In this article, the research progress of graphene and its derivatives based EM absorbers are introduced and the future development of graphene EM absorbing devices are also discussed.

Keywords: graphene; reduced graphene oxide; electromagnetic; absorber

1. Introduction

Graphene is a two-dimensional (2D) material exhibiting an ambipolar electrical field effect [1]. For a long time in history, 2D materials with single-atom thickness like graphene were theoretically predicted as thermodynamically unstable due to the strong thermal fluctuations. In 2004, Andrei Geim and Kostya Novoselov from University of Manchester experimentally proved the existence of graphene with samples achieved with the scotch tape method [1]. Since then, a series of 2D materials such as hBN [2] and silicene [3] were also synthesized. On one hand, the ultrahigh carrier mobility of graphene, far beyond any other semiconductors, makes it an ideal channel material for the development of high-speed field-effect transistors [4]. On the other hand, the strong electrical field effect of graphene can be implemented to realize reconfigurable electromagnetic (EM) devices [5–7].

According to Kubo's formula, the conductivity of graphene (σ_s), consisting of both intraband and interband terms, is calculated as [8]

$$\sigma_s = \sigma_{intra} + \sigma_{inter}, \quad (1)$$

where

$$\sigma_{intra} = \frac{e^2 k_B T}{\pi \hbar^2 (j\omega - 2\tau)} \times \left(\frac{|E_F|}{k_B T} + 2 \ln \left(e^{-\frac{E_F}{k_B T}} + 1 \right) \right), \quad (2)$$

$$\sigma_{inter} = \frac{e^2}{4\pi \hbar} \times \ln \left(\frac{2|E_F| - (\omega - 2j\Gamma) \hbar}{2|E_F| + (\omega - 2j\Gamma) \hbar} \right). \quad (3)$$

e is the elementary electron charge, k_B is the Boltzmann constant, T is the temperature, \hbar is the reduced Planck's constant, ω is the angular frequency, Γ is the carrier scattering rate and E_F is the chemical potential. For frequency below 10 THz, the intraband term dominates, hence $\sigma_{total} \approx \sigma_{intra}$. The chemical potential E_F can be tuned through chemical or electrostatic doping. The electrostatic doping is achieved by sandwiching a dielectric layer between graphene and a conductive (e.g., metal) electrode. When the bias voltage is applied between graphene and the electrode, the carriers (i.e., holes or electrons) are injected into (or extracted from) graphene, resulting in a varying σ_s against the variation of bias voltage. It is noted that a strong electric field in the range of V/nm is usually required in electrostatic doping, resulting in a dielectric layer with thickness varying from several to at most a few hundred nanometers under a practical bias voltage.

Over the past decade, graphene-based waveguide modulators operating at optical frequencies have been reported [9–11]. In addition, graphene-based beam-steering devices operating at mid-infrared frequency have also been proposed, demonstrating effective control over the reflection angle of the incident wave [12,13]. Moreover, graphene and its derivatives such as reduced graphene oxide (rGO) have also been utilized along with other materials to realize EM absorbers with fixed wave absorption and operation frequencies [14–19]. Meanwhile, graphene-based reconfigurable EM absorbers have also been proposed, paving the way for the development of smart EM absorbing materials. [20–31]. Generally, there are two types of graphene EM absorbers, namely, quarter-wavelength absorber and metasurface absorber. As they exhibit different EM absorption performance, the graphene-based quarter-wavelength and metasurface absorbers are introduced separately in this work.

2. Graphene-Based Quarter-Wavelength Absorbers

Quarter-wavelength absorber is a type of EM absorbing material/device with a thickness of $\lambda/4$ or $N \cdot \lambda/4$, where λ is the wavelength in the material and N is a positive integer. The most famous quarter-wavelength absorbers are Salisbury screen [32], Jaumann [33] and Dällenbach absorbers [34]. Although their physical geometries are different from each other, they share an identical wave absorbing mechanism during the operation.

2.1. Graphene-Based Salisbury and Jaumann Absorbers

In the 1940s, Winfield W. Salisbury invented an absorbent structure, known as Salisbury screen, to reduce the radar cross section of EM waves. However, the work was not patented until 1952 due to the security requirements in World War II [32]. The EM absorber consists of a thin resistive layer, a low loss/lossless dielectric spacer and a metallic ground [32]. The resistive layer splits the incidence into reflected and transmitted signals. The metallic ground acts as a perfect reflector that fully reflects the transmitted signal. The thickness of spacer is carefully selected so that destructive wave interference can be achieved between the reflections from resistive sheet and metallic ground. For a spacer with thickness $d = M \cdot \lambda/4$ where M is a positive odd integer, the reflected waves exhibit a phase difference of $M \cdot \lambda/2$ and cancel each other when their amplitude matches. This configuration is also known as a Fabry–Perot resonator, which operates within a narrow frequency range near the resonant frequency.

According to the transmission line theory, the input admittance ($Y_{1,in}$) of Salisbury screen under normal incidence for both transverse electric (TE) and transverse magnetic (TM) polarized waves is [35]:

$$Y_{1,in} = Y_s - jY_d \cot(\beta_d d), \quad (4)$$

where $Y_s = 1/\sigma_s$, $\beta_d = \omega\sqrt{\epsilon_r}/c$, ϵ_r is the relative permittivity of the dielectric spacer, c is speed light, $Y_d = \sqrt{\epsilon_r}/Z_0$ and $Z_0 = \sqrt{\mu_0/\epsilon_0}$ is the free space impedance. To enhance the operation bandwidth of Salisbury screen, a few resistive layer/spacer pairs can also be stacked on the top of each other

to realize the Jaumann absorber, as shown in Figure 1a,b. For a Jaumann screen consisting of N quarter-wavelength-thick layers, the corresponding input admittance can be calculated as [35]

$$Y_{i,in} = Y_s + Y_d \frac{Y_{i-1,in} + jY_d \tan(\beta_d d)}{Y_d + jY_{i-1,in} \tan(\beta_d d)} \quad (i = 1, 2, \dots, N). \quad (5)$$

Thus, the reflection coefficient (Γ_r) can be achieved as

$$\Gamma_r = \frac{Z_{in} - Z_0}{Z_{in} + Z_0}, \quad (6)$$

and the reflectance (R) can be represented as $R = \Gamma_r^2$. Hence, the absorption (A) is

$$A = 1 - R - T, \quad (7)$$

where T is the transmittance. Since the metallic ground fully reflects the signal through the resistive layer(s) and results in zero transmittance (i.e., $T = 0$), Equation (7) can be rewritten as

$$A = 1 - R. \quad (8)$$

That means the wave is either absorbed or reflected in the Salisbury screen and Jaumann absorbers. For $Z_{in} = Z_0$, perfect absorption is achieved as $R = 0$ and $A = 1$. Hence, in practice, engineers always would like to reduce the value of R for absorbers with metallic ground. At microwave frequencies, the return loss (dB), defined as

$$RL = -20 \log |\Gamma_r|, \quad (9)$$

is often preferred over R to describe the reflection of a device. For absorbers with metallic ground, the effective wave absorption is frequently defined as $RL \leq -10$ dB, which means that more than 90% of the signal energy is absorbed.

In 2013, theoretical exploration results on the graphene-based tunable Salisbury screen [36] and Jaumann [37] absorbers operating at THz frequencies were reported. The next year, experimental results of graphene-based transparent Salisbury screen and Jaumann absorbers operating at millimeter wave frequency were presented by Wu et al. [35]. As shown in Figure 1c, their graphene is synthesized on the Cu/SiO₂/Si wafers with over 90% monolayer coverage utilizing chemical vapour deposition (CVD) approach. This is followed by coating a layer of poly (methyl methacrylate) (PMMA) on the top of graphene. Then, the substrate is etched away in the aqueous ammonium persulfate solution, leaving only floating graphene-PMMA films that can be washed in de-ionized water and transferred onto arbitrary substrate. Finally, the PMMA is removed with acetone, leaving only graphene on the new substrate. To reduce the sheet resistance (R_s) of the graphene, they utilize multilayer graphene in the absorber by stacking the graphene-PMMA film on the top of monolayer graphene synthesized on Cu/SiO₂/Si and repeating the etch-and-transfer step. As the thickness of multilayer graphene is negligible, the differences between mono- and multilayer graphene in this work is reflected by the transmittance of optical light, as shown in Figure 1d. The Salisbury screen absorber, utilizing $d = 1.3$ mm and $\epsilon_r = 3.8$ quartz spacer, resonates at a fundamental frequency near 29.6 GHz. The corresponding reflection loss varies with the number of stacked graphene layers at the 5th harmonic frequency as shown in Figure 1e. To enhance its operation bandwidth, a few graphene/quartz pairs are also stacked on the top of each other to realize the Jaumann absorber and the $n = 5$ device demonstrates effective wave absorption over a wide frequency range (125–165 GHz), as shown in Figure 1f. Except increasing the number of graphene layers, Jeong et al. also proposed a graphene-based Salisbury screen for THz frequencies, where chemical doping is implemented to reduce the sheet resistance of their multilayer graphene [38]. As the millimeter thick dielectric spacers are used in the Salisbury and Jaumann absorbers mentioned above, it is difficult to apply electrostatic doping to the graphene layer. Hence, these absorbers operate with fixed absorption and frequencies.

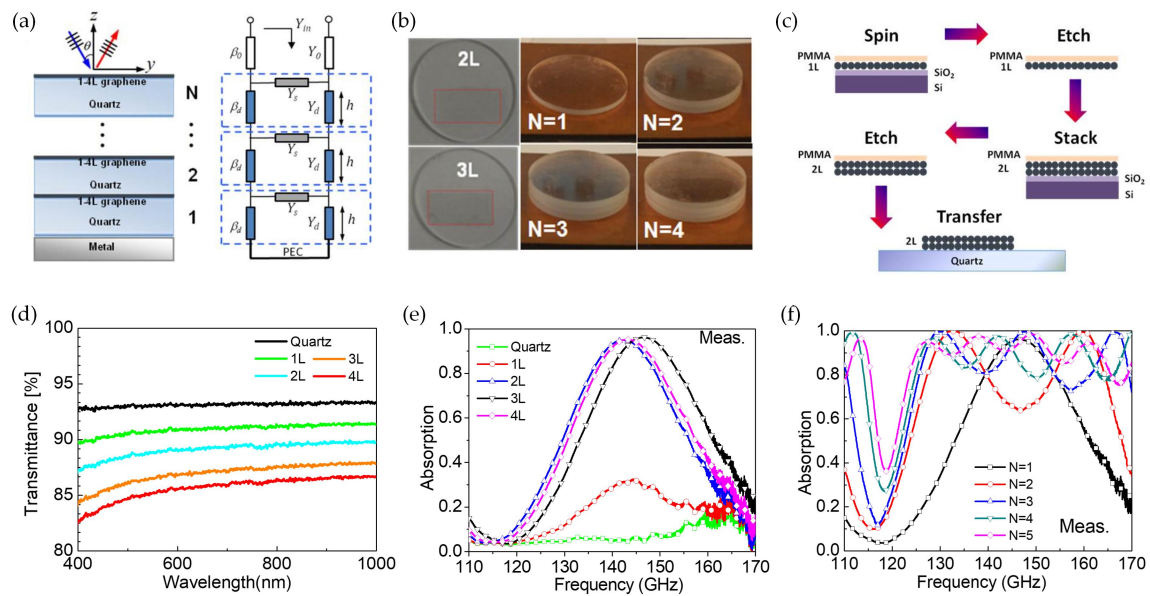


Figure 1. (a) schematic of a N -unit Jaumann absorber and the corresponding transmission-line model; (b) images of graphene–quartz samples with bilayer (2 L) and trilayer (3 L) graphene as well as one to four stacked samples over the metallic ground; (c) fabrication procedure of a 2 L graphene–quartz sample; (d) UV-Vis spectra of the bare quartz and 1 L–4 L graphene–quartz samples; (e) measured absorption spectra of graphene Salisbury screens with bare quartz and 1 L–4 L graphene–quartz samples; (f) measured absorption spectra of graphene Jaumann absorbers with $N = 1$ –5; reprinted with permission from Ref. [35].

To achieve a tunable Salisbury screen, ionic liquid (or gel) is utilized to provide more effective gate control over the traditional dielectric gates in a graphene capacitor structure as shown in Figure 2a,b. For the ionic liquid sandwiched between two graphene/dielectric layers, when a bias voltage is applied, the electrons inside the liquid tend to move and accumulate on the anode graphene layer. The ions with positive charges, on the other hand, move in the opposite way and accumulate on the cathode graphene layer. Thus, the graphene layers on both sides are doped and R_s can vary significantly when a small bias voltage is applied. The thickness of ionic liquid is usually within a few tens of micrometers (e.g., 50 μm) and a bias voltage as low as ± 3.5 V can be used for effective control [39]. By replacing the resistive layer with flexible graphene capacitor, tunable Salisbury screen absorbers operating at microwave [39] and THz [40] frequencies have been experimentally investigated. Under normal incidence, the graphene Salisbury screen in [39] demonstrates tunable wave absorption between 3 dB to 60 dB at 10.5 GHz while the bias voltage varies between 0 V to -1.5 V, as shown in Figure 2c. In Ref. [40], one of the graphene electrodes is replaced by the gold ground and a 20 μm thick porous membrane with ionic liquid soaked inside is sandwiched between the electrodes. Thanks to the reduced thickness of the dielectric spacer (i.e., porous membrane), switchable absorption performance is achieved at 2.83 THz under an incident angle of 30° when the bias voltage varies between 0 V to 2 V, as shown in Figure 2d,e. In addition, the ionic liquid can also be used in a top-gate biased absorber operating at infrared frequencies, as shown in Figure 2c [41]. The device demonstrates a maximum normalized differential reflectance (i.e., $\Delta R/R$) of 0.042, where R is the reflectance at $E_F = 0$ and ΔR is the reflectance variation when $E_F \neq 0$. This graphene Salisbury screen demonstrates poor absorbing performance at infrared frequencies due to the Drude-like behavior of free electrons in graphene [42].

Although the tunable graphene Salisbury screen absorbers have demonstrated excellent switching performance at microwave and THz frequencies, the volatile ionic liquid used for electrostatic doping has to be properly packaged to avoid evaporation. In fact, as an important figure of the ionic liquid based absorbers, the device life has not been systematically investigated. Hence, there is still a long way to go until the packaging technology of ionic liquid is improved for a long life Salisbury screen.

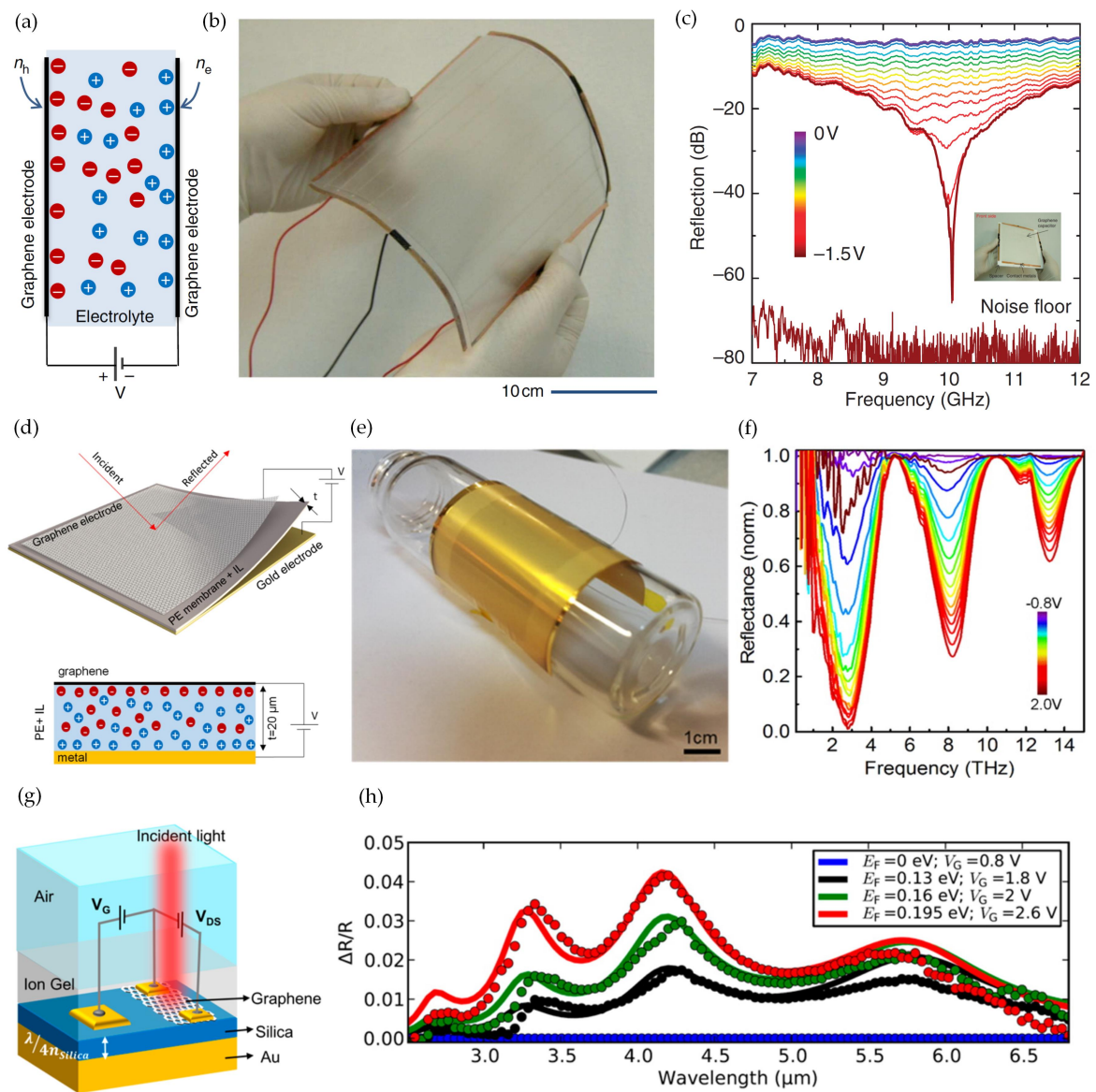


Figure 2. (a) schematic of a graphene capacitor with ionic liquid (or gel) and two graphene electrodes; (b) image of a graphene capacitor; (c) measured reflection spectra of the graphene capacitor based tunable Salisbury screen under various bias voltages, reprinted with permission from [39]; (d) schematic of ionic liquid based graphene Salisbury screen; (e) image of the flexible graphene capacitor based tunable Salisbury screen coated on the surface of a cylindrical object; (f) measured reflection spectra of the flexible Salisbury screen under various bias voltages, reprinted with permission from [40]; (g) schematic of the graphene Salisbury screen with ionic gel based top gate; (h) measured (dotted line) and simulated (solid line) normalized differential reflectance $\Delta R/R$ vs. frequency under various bias voltages, where R is the reflectance of the device when $E_F = 0$ and ΔR is the reflectance variation from R when $E_F \neq 0$, reprinted with permission from [41].

2.2. Graphene and Its Derivatives-Based Dällenbach Absorbers

Unlike the Salisbury and Jaumann screens that require resistive layer and low loss/lossless dielectric spacer over a metallic ground, the Dällenbach absorber utilizes a lossy homogeneous material with complex relative permittivity $\epsilon_r = \epsilon' - j\epsilon''$ and permeability $\mu_r = \mu' - j\mu''$ above the metallic layer [34]. The EM wave absorption of Dällenbach layer can also be illustrated with the transmission line theory. The corresponding input impedance for normal incidence is derived as

$$Z_{in} = Z_0 \sqrt{\frac{\mu_r}{\epsilon_r}} \tanh \left[j \left(\frac{2\pi f d}{c} \sqrt{\mu_r \epsilon_r} \right) \right]. \quad (10)$$

Hence, the absorption and return loss can also be calculated with Equations (8) and (9).

In addition to the wave cancellation at the interface when $d = M \cdot \lambda/4$, the Dällenbach absorber also exhibits magnetic and/or electrical conduction loss that enhance the EM wave absorption performance such as peak absorption rate and effective absorption bandwidth. The corresponding magnetic and electrical loss can be determined by the magnetic ($\delta_m = \mu''/\mu'$) and electrical ($\delta_e = \epsilon''/\epsilon'$) loss tangent. It is noted that both ϵ_r and μ_r play important roles in the EM wave absorption. In order to characterize the matching between ϵ_r and μ_r , a factor $|\Delta|$ is proposed [43]

$$|\Delta| = |\sinh^2(Kfd) - M|, \quad (11)$$

where

$$K = \frac{4\pi \sqrt{\mu_r' \epsilon_r'} \sin\left(\frac{\delta_e + \delta_m}{2}\right)}{c \cos(\delta_e) \cos(\delta_m)}, \quad (12)$$

and

$$M = \frac{4\mu_r' \epsilon_r' \cos(\delta_e) \cos(\delta_m)}{(\mu_r' \cos(\delta_e) - \epsilon_r' \cos(\delta_m))^2 + \left[\tan\left(\frac{\delta_m - \delta_e}{2}\right) \right]^2 (\mu_r' \cos(\delta_e) + \epsilon_r' \cos(\delta_m))^2}. \quad (13)$$

For matched impedance, $|\Delta|$ approaches zero and excellent absorption is achieved. When $|\Delta|$ is away from zero, poor impedance matching is observed and the absorption performance is degraded.

To achieve a Dällenbach absorber, graphene and its derivatives such as rGO are often mixed with non-magnetic (i.e., $\mu' \approx 0$ and $\mu'' \approx 1$) [44–46] or magnetic [47] materials to form lossy composites. In 2011, Bai et al. investigated the microwave absorbing properties of rGO/poly-(ethylene oxide) (PEO) composites based Dällenbach layer [44]. Due to the high electrical conduction loss and other losses result from dielectric relaxation, interface scattering, etc. as well as the wave cancellation at the material/air interface, excellent microwave absorption performance is achieved. For a thickness of 1.8 mm, the material demonstrates a minimum RL (RL_{\min}) of -38.8 dB at 16.4 GHz with more than 4.1 GHz effective absorption bandwidth (13.9–18+ GHz).

In 2012, the microwave absorption of composites consist of rGO and nitrile butadiene rubber (NBR) were conducted by Singh et al. [45]. The non-magnetic rGO/NBR Dällenbach absorber exhibits a RL_{\min} as low as -57 dB and 4.5 GHz effective absorption bandwidth with a thickness of 3 mm. The authors believe the multiple reflections inside the rGO/NBR composites as well as the ionic conduction and dipolar relaxation caused by microwave/material interaction are the possible reasons behind the enhanced peak absorption.

In 2013, Liu et al. synthesized the non-magnetic polypyrrole (PPy)/rGO/Co₃O₄ nanocomposites with a three-step approach [46]. They explored the complex permittivity and permeability of the synthesized PPy/rGO/Co₃O₄ nanocomposites and revealed that dielectric loss plays an important role in microwave absorption. With a thickness of 2.5 mm, the Dällenbach absorber exhibits a broad effective absorption bandwidth of more than 6.7 GHz (11.6–18+ GHz) and a RL_{\min} of -33.5 dB at 13.8 GHz.

In 2015, Zhang et al. investigated the microwave absorbing performance of a Dällenbach absorber with ultralight compressible graphene foam (GF) [48]. Figure 3a–d illustrate the cross-sectional SEM images of uncompressed GF and GF under 30% (GF-30), 60% (GF-60) and 90% (GF-90) compressive strains. Figure 3e depicts the schematic of corresponding Dällenbach absorber. The measured real permittivity and loss tangent are shown in Figure 3f,g. Although the unstrained GF with 10 mm thickness is required and the RL_{\min} achieved is only -28 dB at 12.2 GHz, the material demonstrates excellent broadband absorption over three different frequency bands, as shown in Figure 3h–j.

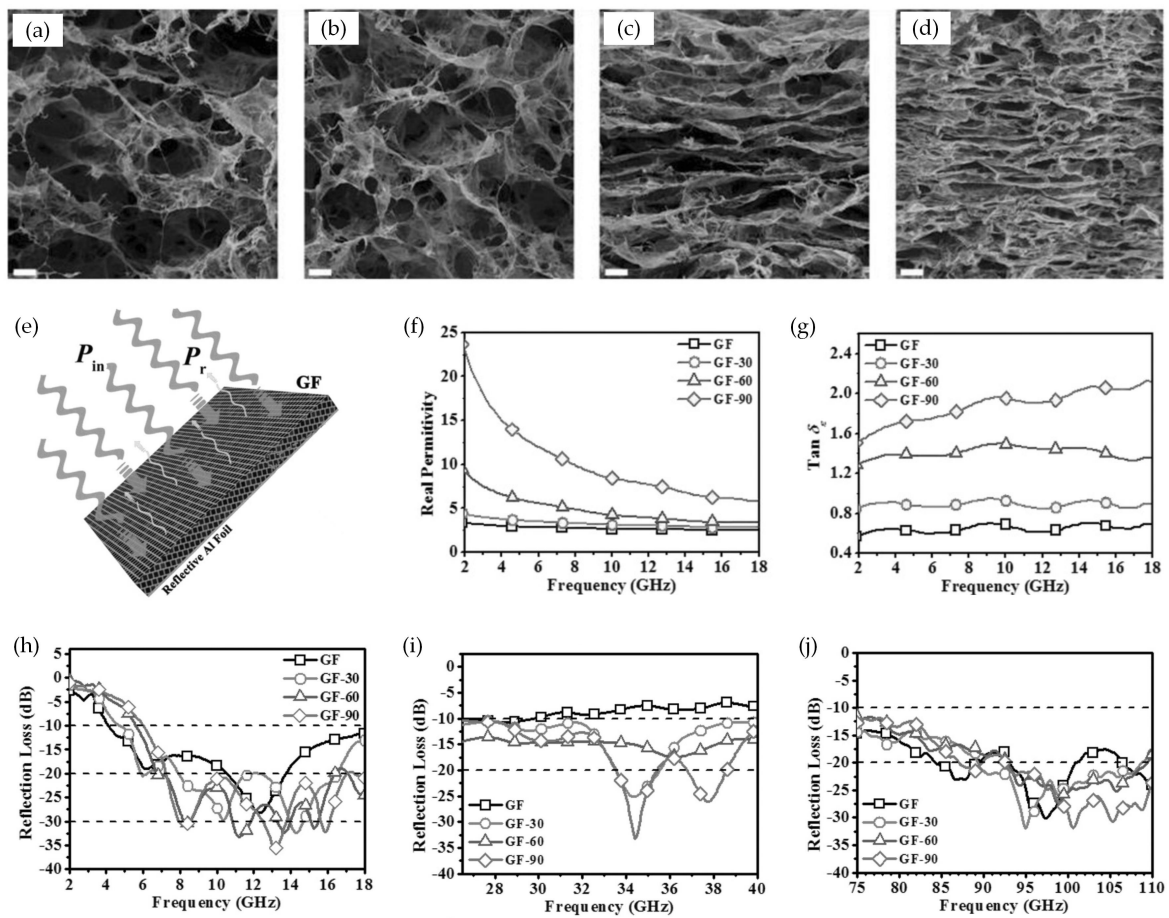


Figure 3. The cross-sectional SEM images of (a) graphene foam (GF) and GF under (b) 30%; (c) 60%; and (d) 90% compressive strains. The length of scale bar is 20 μm ; (e) the schematic of GF Dallenbach absorber. The measured electrical properties of GF-30, GF-60 and GF-90: (f) the real part of complex permittivity; (g) the loss tangent. The measured return loss (RL) spectra of GF-30, GF-60 and GF-90 for (h) 2–18 GHz; (i) 26.5–40 GHz and (j) 75–100 GHz, reprinted with permission from Ref. [48].

In 2016, Ameer et al. combined the magnetic NiFe_2O_4 nanoparticles and nanohybrids with non-magnetic rGO sheets to realize a Dallenbach layer operating at low microwave frequencies [47]. The calculated RL demonstrates two absorption peaks within 1 MHz to 3 GHz ($\text{RL}_{\text{min}} = 68$ dB at 1.11 GHz) and an effective operation bandwidth of 3 GHz or more under a thickness of 2 mm only. In the same year, Han et al. reported their exploration results on rGO/Silicon oxycarbide (SiOC) based EM absorbing material [49]. Figure 4a–f present the SEM images of the rGO/SiOC ceramic. A remarkable $\text{RL}_{\text{min}} = -69.3$ dB is achieved at 10.55 GHz for a Dallenbach absorber with thickness of 2.35 mm, as shown in Figure 4g. In addition, they also explore the temperature-dependent complex permittivity of the rGO/SiOC composites from 293–673 K. It is noted that both ϵ' and ϵ'' increase when the temperature rises, as shown in Figure 4h,i, resulting in smaller RL_{min} and thinner absorber thickness.

In 2017, a double-layer Dallenbach absorber consists of a matching layer (i.e., $\text{Co}_{0.2}\text{Ni}_{0.4}\text{Zn}_{0.4}\text{Fe}_2\text{O}_4$) on the top and a absorption layer (i.e., rGO) underneath was investigated [50]. The input impedance is calculated as

$$Z_{in} = \frac{\sqrt{\frac{\mu_2}{\epsilon_2}} \left(\sqrt{\frac{\mu_1}{\epsilon_1}} \tanh \left[j \left(\frac{2\pi f d_1}{c} \right) \sqrt{\mu_1 \epsilon_1} \right] + \sqrt{\frac{\mu_2}{\epsilon_2}} \tanh \left[j \left(\frac{2\pi f d_2}{c} \right) \sqrt{\mu_2 \epsilon_2} \right] \right)}{\sqrt{\frac{\mu_2}{\epsilon_2}} + \sqrt{\frac{\mu_1}{\epsilon_1}} \tanh \left[j \left(\frac{2\pi f d_1}{c} \right) \sqrt{\mu_1 \epsilon_1} \right] \tanh \left[j \left(\frac{2\pi f d_2}{c} \right) \sqrt{\mu_2 \epsilon_2} \right]}, \quad (14)$$

where μ_1 and ϵ_1 are the complex relative permeability and permittivity of absorption layer, and μ_2 and ϵ_2 are the complex relative permeability and permittivity of matching layer. d_1 and d_2 are the thicknesses of absorption and matching layers, respectively. The corresponding RL is calculated with Equations (6) and (9). A Peak absorption of -52.2 dB is achieved at 10 GHz for the proposed bilayer Dällenbach absorber and the effective absorption bandwidth is as broad as 10 GHz (6.4–16.4 GHz) for an overall material thickness of 4 mm ($d_1 = 1.4$ mm and $d_2 = 2.6$ mm).

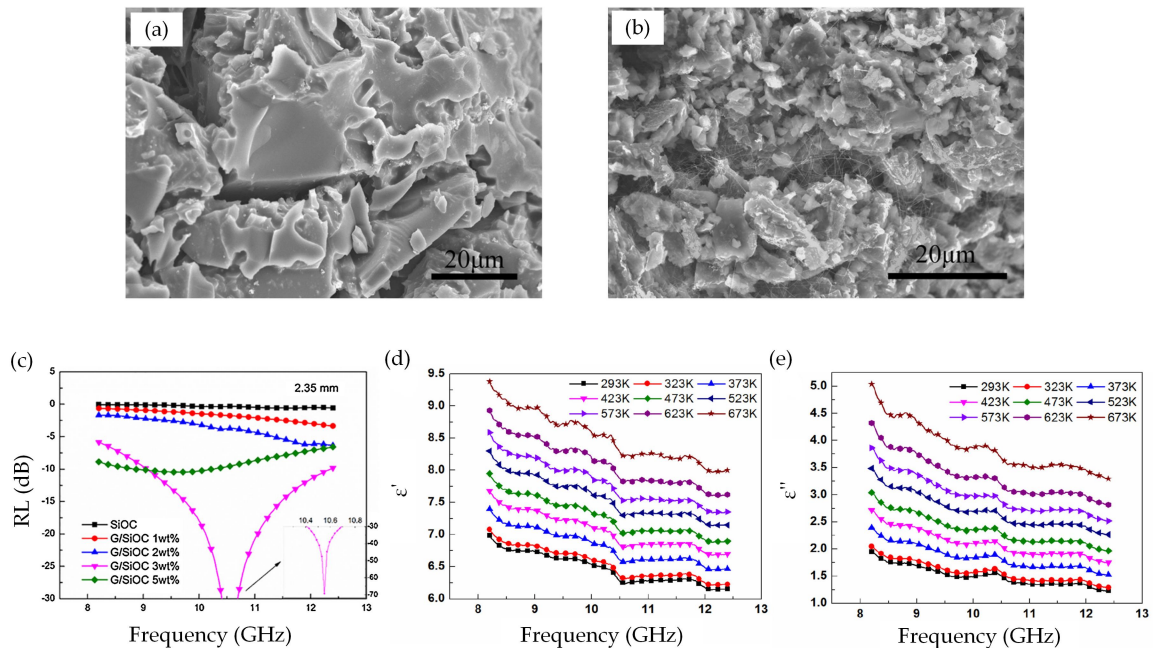


Figure 4. The SEM images of (a) SiOC ceramic and (b) G/SiOC ceramic; (c) the calculated RL spectra of Dällenbach absorber with G/SiOC synthesized under various amounts of graphene oxide. The measured (d) real and (e) imaginary parts of complex permittivity under various temperatures, reprinted with permission from Ref. [49].

Table 1 summarizes the performance of graphene or its derivatives based Dällenbach absorbers as well as the corresponding absorber thickness. It is noted that the RL of most devices are calculated utilizing the measured ϵ_r and/or μ_r rather than achieved from an actual S-parameter measurement. Hence, the correction of the calculated RL heavily depends on the accuracy of the extracted ϵ_r and/or μ_r . What is worse, as the input impedance of Dällenbach absorber given by Equation (10) is derived for homogeneous material above the metallic layer, the homogeneity of composites can also affect the RL and substituting the measured effective ϵ_r and/or μ_r into Equation (10) may not correctly predict the input impedance of the absorber. Last but not least, the effect of incident angle is rarely investigated for the graphene Dällenbach absorbers. As most of them operate at microwave frequencies aiming to reduce the radar cross section for military applications, it is highly desired to achieve effective wave absorption in a wide incident angle. Therefore, further experimental explorations are required to validate the absorption performance of the graphene Dällenbach absorbers.

Table 1. Microwave absorption properties of graphene and its derivatives based composites. (BW: bandwidth; RL: return loss)

Year	Ref.	Type	BW _{max} (GHz)	t _{max} (mm)	RL _{min} (dB)	f _{min} (GHz)	t _{min} (mm)
2018	[51]	rGO/FeNi	5.6 (10.9–16.5)	2	−42.6	14.3	1.5
2018	[52]	rGO/MWCNTs/ZnFe ₂ O ₄	>2.3 (15.7–18+)	1	−22.2	17.4	1
2018	[53]	Graphene/CoFeAl-LDH	7.36 (10.4–17.76)	2.5	−23.8	14.2	2.5
2017	[18]	rGO/SiC	>4.2 (8.2–12.4+)	3.7	−40.7	10.9	3.5
2017	[50]	rGO/Co _{0.2} Ni _{0.4} Zn _{0.4} Fe ₂ O ₄	10 (6.4–16.4)	4	−52.2	13.5	4
2017	[54]	rGO/CoFe ₂ O ₄	5 (12.2–17.2)	2	−53.6	11.4	2.5
2017	[55]	rGO/FeNi/CS	5 (13–18)	1.5	−45.2	15	1.5
2017	[56]	rGO/ZnO	>4.2 (8.2–12.4+)	4.8	−27.8	9.57	4.8
2017	[57]	Graphene/NiO	4.24 (12.48–16.72)	1.7	−59.6	14.16	1.7
2016	[47]	rGO/NiFe ₂ O ₄	>3 (0.01–3+)	2	−68	1.11	2
2016	[49]	Graphene/SiOC	3.9 (8.2–12.1)	2.65	−69.3	10.55	2.35
2016	[58]	Graphene/PANI/TiO ₂	4.4 (12.2–16.6)	1.5	−45.4	14.4	1.5
2016	[59]	Graphene/Fe ₃ O ₄ /Fe	6.2 (11.8–18)	2	−58	5.2	4.6
2015	[48]	Graphene Foam	>14 (4–18+)	10	−28	12.2	10
2015	[60]	GNSs/rGO-CoFe ₂ O ₄	>4.2 (8.2–12.4+)	2.5	−21.8	11.8	1.25
2015	[61]	rGO/HGS	4.1 (13.1–17.2)	2	−46	10.9	2
2014	[62]	rGO/FeNi	3.3 (11–14.3)	1.5	−32	12.4	1.5
2014	[63]	Graphene/Fe ₃ O ₄ /SiO ₂ /NiO	5.1 (12.4–17.5)	1.8	−51.5	14.6	1.8
2014	[64]	rGO/ZnO	6.3 (11.7–18)	2.5	−25.95	10.2	3
2013	[46]	rGO/PEDOT/Co ₃ O ₄	3.1 (9.4–12.5)	2	−51.1	10.7	2
2013	[65]	Graphene/Fe	4.4 (9.7–14.1)	2	−45	7.1	3
2013	[66]	rGO/CuS/PVDF	3.8 (8.9–12.7)	2.5	−32.7	10.7	2.5
2013	[67]	rGO/Fe ₃ O ₄	2.8 (10.4–13.2)	2	−26.4	5.3	4
2013	[68]	Graphene/Co ₃ O ₄	>6.4 (11.6–18+)	2.5	−33.58	15.8	2.5
2013	[69]	Graphene/Fe ₃ O ₄	5 (10.8–15.8)	3	−40.3	7.04	5
2012	[45]	rGO/NBR	4.5 (7.5–12)	3	−57	9.6	3
2012	[70]	Graphene/PANI	5.6 (10.5–16.1)	2.5	−45.1	12.9	2.5
2012	[71]	rGO/Fe ₃ O ₄	4.9 (10.8–15.7)	2	−24	12.9	2
2011	[44]	rGO/PEO	>4.1 (13.9–18+)	1.8	−38.8	16.4	1.8

MWCNT: multiwall carbon nanotube; LDH: layered double hydroxide; CS: carbon spheres; SiOC: silicon oxycarbide; PANI: polyaniline; GNS: graphene nanosheet; HGS: hollow glass spheres; PEDOT: poly(3,4-ethylenedioxythiophene); PVDF: polyvinylidene fluoride; NBR: nitrile butadiene rubber; PEO: poly(ethylene oxide).

2.3. Dielectric/Graphene Multilayer Absorbers

Finally, there are also quarter-wavelength absorbers based on dielectric/graphene structure operating from THz to optical frequencies under wide absorption angle [72–77]. Unlike the Salisbury, Jaumann and Dällenbach absorbers that require a metallic ground, the dielectric/graphene absorbers utilize one or more kinds of dielectrics as well as graphene to achieve EM absorption, as shown in Figure 5a–c. Slightly different from the absorbers with a metallic ground, the EM wave transmittance (T) has to be considered in these devices and the absorption (A) is calculated with Equation (7). Strong wave absorption is achieved when the transmittance is minimized and Fabry–Perot resonance occurs. The absorption performance of dielectric/graphene absorbers can also be tuned by varying the chemical potential of graphene [75–77]. No extra metallic electrodes are required in these devices as the graphene layers act as optical transparent electrodes for self-biasing, as shown in Figure 5b,c.

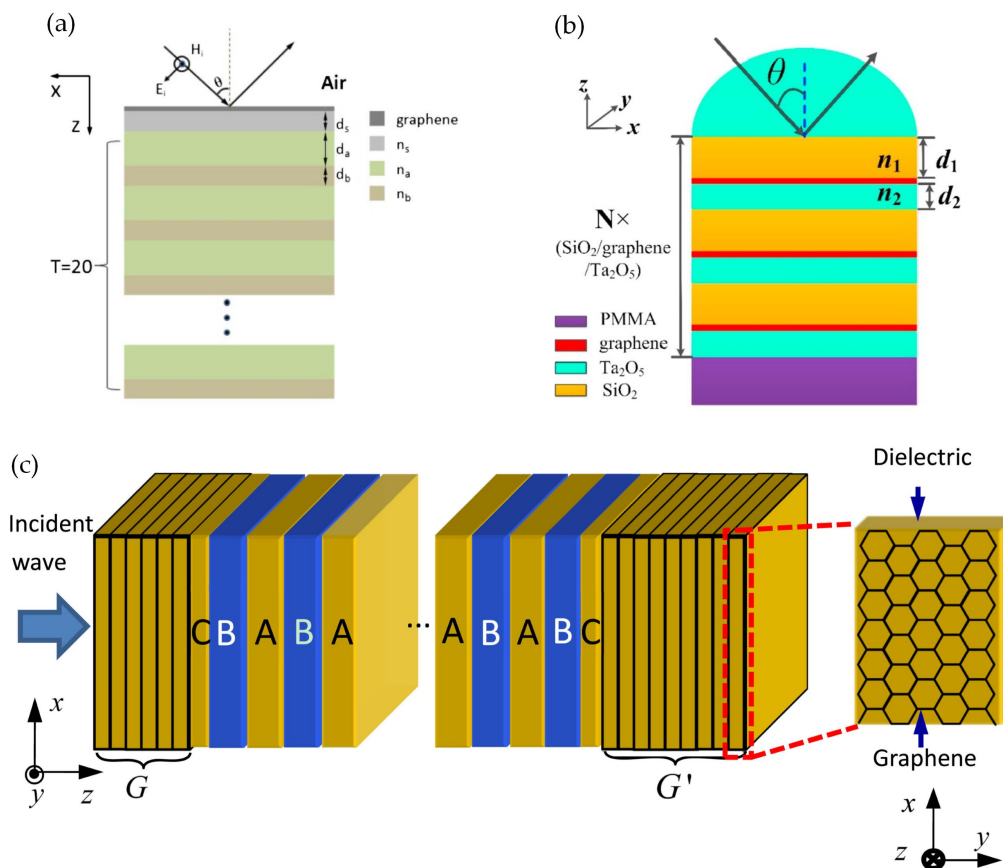


Figure 5. (a) schematic of THz absorber with graphene on the top and periodically stacked dielectric layers with refractive indexes n_s , n_a and n_b respectively, reprinted with permission from Ref. [74]; (b) schematic of electromagnetic (EM) absorber operating at visible and near-infrared frequencies with periodically stacked SiO₂/graphene/Ta₂O₅ layers on poly (methyl methacrylate) (PMMA), reprinted with permission from Ref. [77]; (c) schematic of THz absorber with GC(BA)^N(AB)^NCG', where N is the number of layers, G and G' consist of stacked graphene/dielectric layers and A, B, C are dielectrics, reprinted with permission from Ref. [75].

Although the simulation results of these devices demonstrate promising wave absorption performance, there are a few challenges that have to be overcome before they can be used in reality. First, the thickness of dielectric layers in each period has to be carefully designed so that the wave experiences a quarter-wavelength path inside the material to ensure good wave cancellation at the interfaces. Consider the devices are usually designed for THz to optical frequencies, the dielectric thickness has to be carefully controlled otherwise the operation frequency can vary significantly from the designed frequency. Second, the dielectric/graphene multilayer absorbers should be financially competitive because there are also alternatives in the market. As these devices share an expensive Complementary Metal Oxide Semiconductor (CMOS)-like top-down fabrication approach, obviously, the most effective way to reduce the manufacturing cost is mass production. To make them financially viable for the consumers, an international market is greatly desired. Finally, since these works are all theoretical explorations, further experimental investigations are required to validate the simulation results.

3. Graphene-Based Metasurface Absorbers

Metamaterials are artificial materials possessing characteristics not found in nature or difficult to obtain naturally. Metamaterials are composed of carefully designed periodic sub-wavelength structures and metasurfaces are two-dimensional metamaterials usually with sub-wavelength thickness. Over the

past few decades, metasurfaces have attracted a great deal of attention due to its potential applications in radar systems, wireless communications, etc. Metasurfaces are usually used to manipulate the EM wave propagation such as EM wave absorbing [78,79] and shielding devices [80–82].

Recently, graphene has been proposed as a tunable material for metasurface design. The graphene-based metasurface absorbers operates with different mechanisms including asymmetric Fabry–Perot [78] and guided mode [83–85] resonances, hyperbolic-type dispersion [86], magnetic [87] and plasmonic [88–91] resonances, etc. The operation frequency of graphene-based metasurface absorbers can vary in a wide range from microwave [92] to optical frequencies [93] with nearly perfect absorption. In addition, since the conductivity of graphene can be controlled by its chemical potential, active graphene-based metasurface absorbers can be realized. The properties of metasurface strongly depend on the design of unit cell. Generally, graphene are used as a continuous layer or patterned structure in metasurface absorbers. On one hand, continuous graphene layer can be combined with patterned metal [94–97] or dielectric layers [21,24,83,98–100] to couple the incident wave into resonant mode. On the other hand, graphene can also be patterned into periodic unit cells to support a single [101] or multiple resonant modes [26,102–104] for EM wave absorption. In some cases, both patterned graphene and metallic structures are utilized in the unit cell design [105,106].

3.1. Multiband and Broadband Operation for Graphene Metasurface Absorbers

Similar to the Salisbury screen, most of the graphene metasurface absorbers also utilize metallic ground that allow almost zero transmittance. Full-wave simulations have been widely used to estimate the performance of graphene metasurface absorber. With carefully designed unit cell structures, a couple of graphene metasurface absorbers with dual resonant modes within THz frequencies have been theoretically investigated [26,107–109]. In 2016, a quad-band THz absorber utilizing a single patterned graphene layer was presented by Masumina et al. The symmetrical unit cell design makes it insensitive to the polarization of EM waves and the simulation results demonstrate excellent wave absorption under an incident angle between 0° to 40° . The next year, Parvaz et al. proposed a penta-band metasurface absorber composed of metallic rings and graphene sheets operating at far-infrared frequencies, as shown in Figure 6a,b [110]. A transmission line model is derived and the calculated results agree excellently with the results achieved from full wave simulations. The absorber exhibits stable wave absorption while the incident angle varies between 0° to 75° for both TE and TM polarized waves.

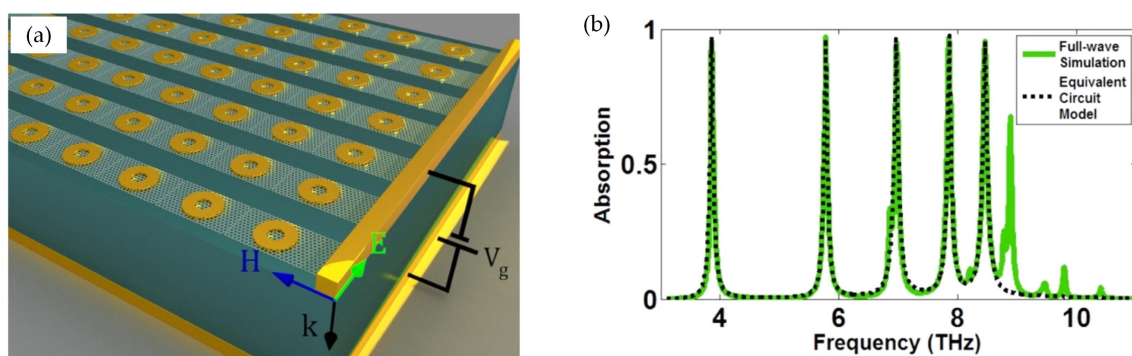


Figure 6. (a) schematic of penta-band graphene metasurface absorber; (b) the absorption spectra achieved with full-wave simulation (green solid line) and equivalent circuit model (black dashed line), reprinted with permission from Ref. [110].

It is noted that, for metasurfaces supporting multiple resonant modes, if the resonant frequencies are designed close enough, the absorption peaks would partly overlap with each other and the device tends to perform as a broadband absorber. For instance, Zhang et al. proposed a graphene metasurface absorber utilizing unit cells consist of three metallic circular patches with different diameters, as shown

in Figure 7a [111]. From the numerical simulation results, it is easy to see that the device resonates at 33.68 THz, 35.90 THz and 39.65 THz, resulting in an enhanced effective absorption bandwidth compared with the device with a single resonant mode. In addition, thanks to the symmetric circles used in the unit cells, the metasurface also demonstrates polarization-insensitive performance over 31.2–37 THz with no less than 90% wave absorption (see Figure 7b). In addition, multiple resonant modes can also be achieved by utilizing the polarization-insensitive dual electric LC (i.e., inductance (L) and capacitance (C)) unit cells, as shown in Figure 7c [95]. Effective wave absorption is achieved within 27.78 THz to 42.16 THz under a wide incident angle (see Figure 7d,e), corresponding to a maximum fractional bandwidth of 41.12% at normal incidence.

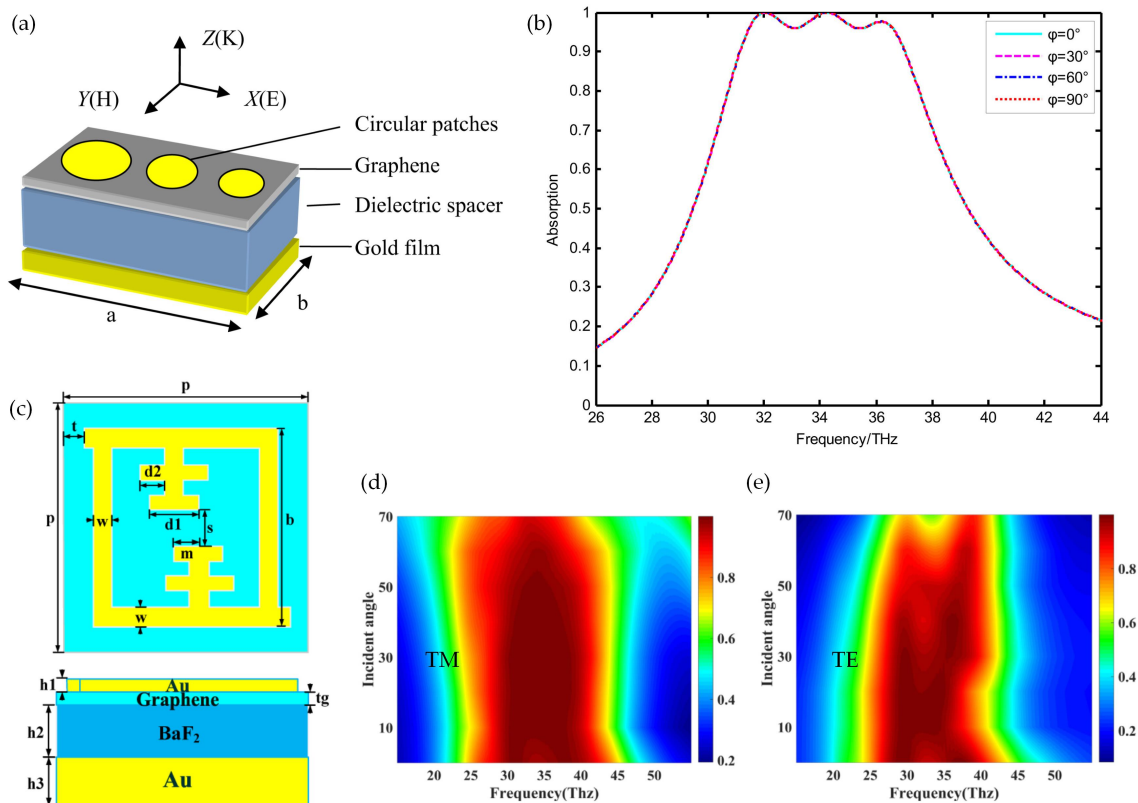


Figure 7. (a) unit cell of broadband graphene metasurface absorber consisting of continuous graphene and three circular metallic patches; (b) simulated absorption spectra with various azimuth angles (φ), reprinted with permission from Ref. [111]; (c) schematic of a dual electric LC (i.e., inductance (L) and capacitance (C)) unit cell; (d) the wave absorption vs. frequency and incident angles for transverse magnetic (TM) polarized waves; (e) the wave absorption vs. frequency and incident angles for transverse electric (TE) polarized waves, reprinted with permission from Ref. [95].

Moreover, it is also possible to achieve broadband THz absorption utilizing a single layer of periodic graphene ribbons with gradient width [112], sinusoidally-patterned graphene sheets [113] and square-patterned graphene [114]. Although asymmetric graphene sheets and ribbons are used for unit cell designs, these absorbers demonstrate polarization-insensitive absorption and small performance variation for incident angles between 0° to 30° . In 2016, Agarwal et al. proposed a broadband absorber with four gold helices buried in the dielectric for each unit cell. Graphene is placed on the top of the metasurface [115], as shown in Figure 8, to enhance the wave absorption and a relative absorption bandwidth of 160% (i.e., for wavelength 200–1792 nm) is achieved. The symmetrical unit cell design also guarantees polarization-independent wave absorption performance over near ultraviolet to near infrared frequency.

In addition, a couple of research groups have also designed broadband graphene metasurface absorbers by stacking multiple metasurfaces resonating at different frequencies on the top of each other [116–121]. In 2016, Huang et al. presented their experimental results on the metasurface printed on a flexible substrate with graphene nano-flakes ink [122]. As shown in Figure 9a–e, the flexible absorber can be easily coated on the surface of a cylindrical object. The measurement results demonstrate effective microwave absorption from 10.4 GHz to 19.7 GHz, corresponding to a fractional bandwidth of 62%.

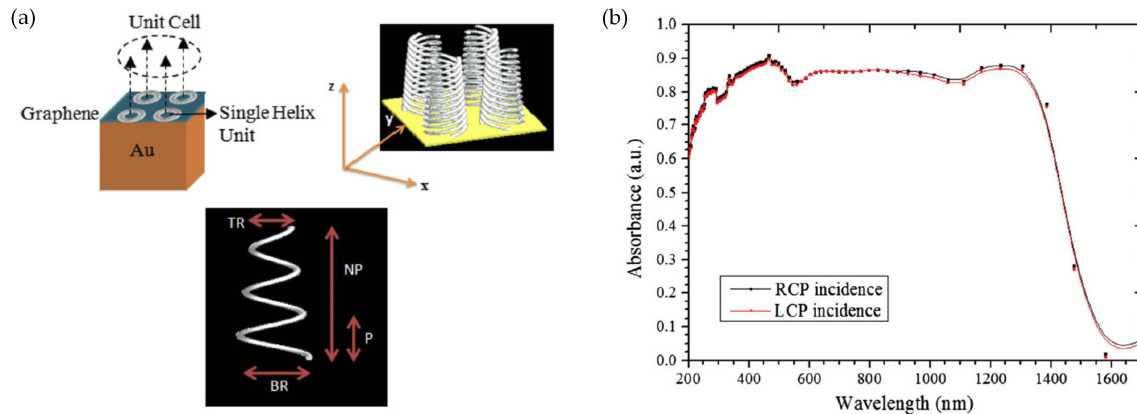


Figure 8. (a) schematic of graphene metasurface absorber with buried metallic helices; (b) the simulated absorption spectra for left- and right-circular polarized waves, reprinted with permission from Ref. [115].

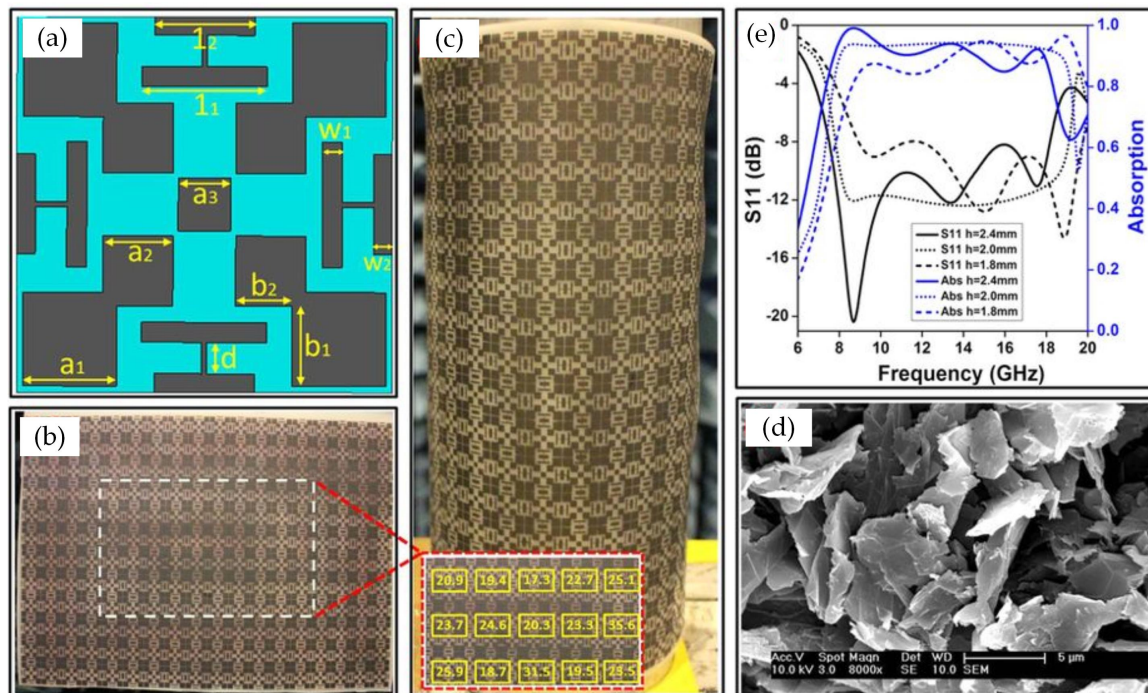


Figure 9. (a) schematic of the unit cell; (b) image of the fabricated absorber; (c) absorber coated on the surface of metallic cylinder; (d) SEM image of the printed graphene; (e) measurement results of the graphene metasurface absorber, reprinted with permission from Ref. [122].

Recently, Ye et al. proposed a frequency selective surface (FSS) based metasurface absorber with a patterned multilayer rGO sandwiched between two glass fiber layers, as shown in Figure 10a [123]. Two absorption peaks are generated in their device, demonstrating broadband wave absorption at microwave frequencies. The measured RL exhibits a minimum of -46 dB at 9.1 GHz for $d_1 = 1.4$ mm and $d_2 = 2.2$ mm. Meanwhile, the device demonstrates excellent microwave absorption ($RL < 10$ dB)

over the whole measurement range (8–18 GHz), as shown in Figure 10b. The authors attribute the advantage of using rGO-FSS to the polarization and conduction losses induced by abundant micro-defects and hopping of charge carriers in their multilayer rGO, respectively.

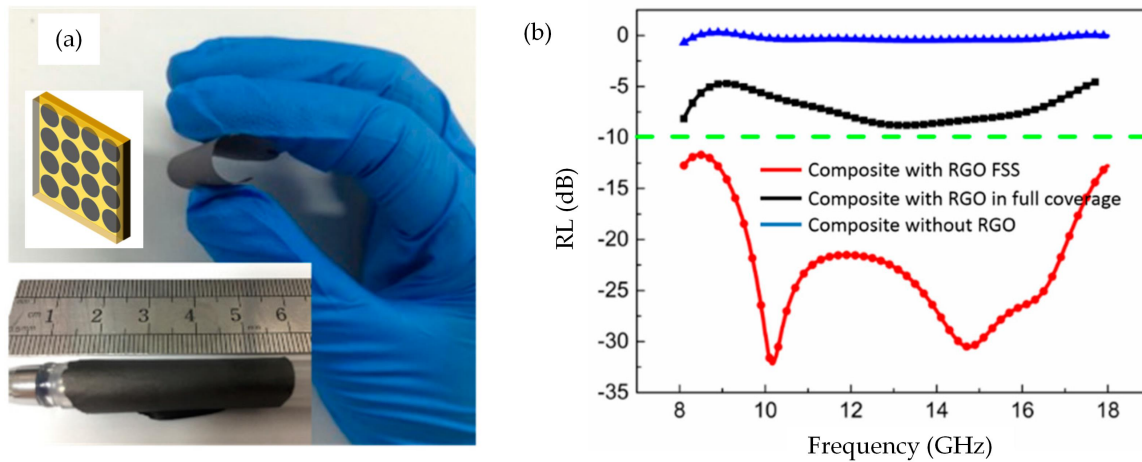


Figure 10. (a) image of the fabricated flexible multilayer (reduced graphene oxide) rGO. The upper inset illustrates the rGO based frequency selective surface (FSS) sandwiched between two dielectric layers and the lower inset demonstrates the dimensional of an unpatterned multilayer rGO; (b) the measured RL spectra without rGO (blue), with rGO in full coverage (black) and with rGO-FSS (red), reprinted with permission from Ref. [123].

Although the operation of broadband graphene metasurface absorbers has been experimentally demonstrated, the tunability of graphene conductivity has not been investigated in these experiments. Due to the tunable sheet resistance of graphene, it is interesting to have a look at the explorations on reconfigurable graphene metasurface absorbers as well.

3.2. Reconfigurability of Graphene Metasurface Absorbers

Thanks to the tunable conductivity of graphene, a large amount of theoretical investigations on tunable graphene metasurface absorbers have been presented in the past few years. By combining the continuous graphene layer with patterned metallic unit cell structures, EM wave absorbers with reconfigurable operation frequency [20,29,31,124] or bandwidth [95,105] can be achieved. The devices with two independently-tunable resonant frequencies at THz [125,126] and mid-infrared [127] frequencies are also explored with full-wave simulations, demonstrating excellent stability on one resonant frequency while the other frequency is tuned. In addition, by varying the chemical potential of graphene, some metasurface absorbers also exhibit switching performance and operate as either fine absorbers or reflectors [104,113,114,128,129]. It is worth mentioning that the thick dielectric layer in the range of micrometers used in some of these theoretical calculations are impractical for electrostatic doping [22,27,28,113]. Furthermore, in some works, the effects of interconnecting wires between unit cells for the implementation of external bias voltage have not been taken into consideration, resulting in great uncertainty in the actual performance of the absorbers [22,28,108,111,129–132].

Beside the theoretical explorations, Yi et al. have also presented their experimental results on metasurface absorbers with square-patterned graphene on PET [133]. By utilizing samples with different R_s or changing the number of graphene/PET layers, the mechanically reconfigurable absorber utilizing tuning surface resistance (TSR) and stacking graphene metasurface (SGM) approaches are experimentally investigated, as shown in Figure 11a–d. Although both TSR- and SGM-type absorbers exhibit narrowband and poor microwave absorptions for normal incident waves, they exhibit mechanically tunable resonant frequency from 12.5 GHz to 13.3 GHz and 12.3 GHz to 13.5 GHz,

respectively. From the comparisons between simulation and experiment results, it is also noted that the gaps resulting from imperfect stacking process increase the resonant frequency of the absorber.

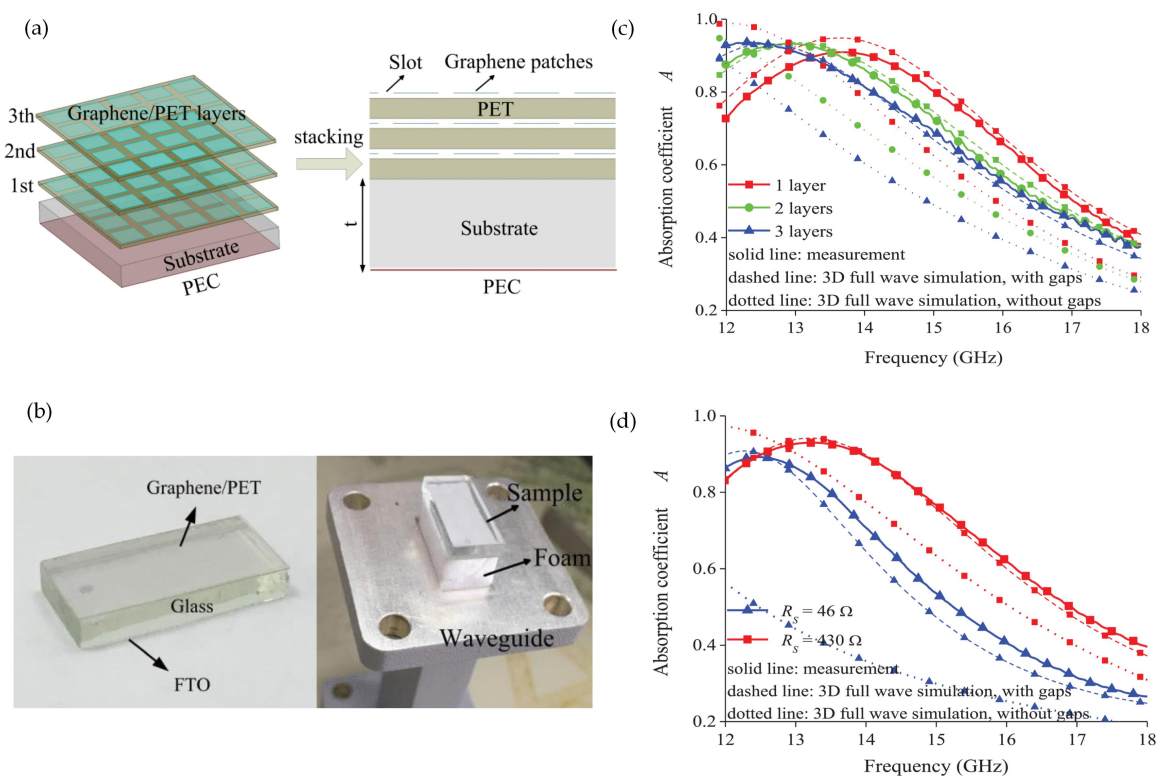


Figure 11. (a) schematic of the multilayer metasurface absorber with square-patterned graphene; (b) fabricated graphene metasurface absorber; (c) the measured absorption spectra for 1–3 stacked square-patterned graphene layers as well as the simulation results with and without gap between the layers; (d) the measured absorption spectra for a single square-patterned graphene layer but with different graphene sheet resistances and the corresponding simulation results with and without gaps between the layers, reprinted with permission from Ref. [133].

In addition, Chen et al. proposed a graphene metasurface absorber operating at microwave frequencies as shown in Figure 12a,d [134]. They sandwich the electrolyte between two PVC supported graphene FSSs and tend to vary the sheet resistance of graphene through electrostatic doping. Although excellent agreement have been achieved between measurement and simulation results for samples with $R_s = 20, 50$ and $70 \Omega/\text{sq}$ under normal incidence, none of their samples exhibit reconfigurable absorption performance that has been predicted by full-wave simulations. The authors attribute the failure of their sample to the hot lamination process that reduces the gap between the graphene layers. Recently, Jiang et al. presented their experimental results on a THz absorber utilizing patterned graphene as unit cells [135]. A narrowband absorption from 1.7 THz to 1.97 THz is experimentally achieved under a bias voltage of 30 V for normal incident wave. Due to the thick dielectric layer ($27 \mu\text{m}$) used for electrostatic doping, the sample exhibits a small absorption performance variation while the bias voltage varies from 0 V to 60 V.

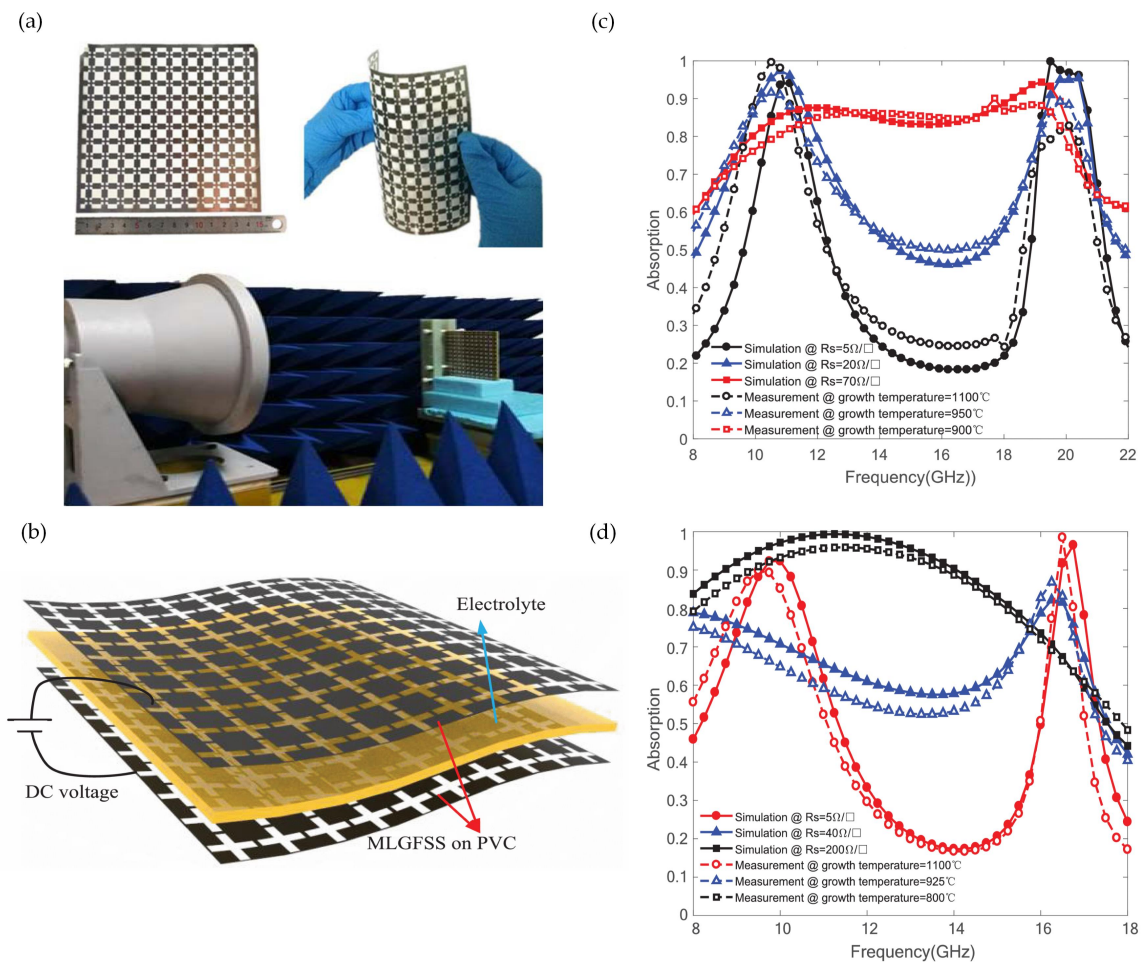


Figure 12. (a) image of the fabricated Type-A sample and measurement setup; (b) measured and simulated absorption spectra of Type-A metasurface with various graphene sheet resistances; (c) schematic of Type-B sample; (d) measured and simulated absorption spectra of Type-B metasurface with various graphene sheet resistances, reprinted with permission from Ref. [134].

4. Conclusions and Outlook

In summary, this work introduces the implementation of graphene and its derivatives in quarter-wavelength and metasurface absorbers for EM wave absorption. The experimental results on narrowband graphene Salisbury screen with electrically tunable absorption strength have been discussed. In addition, graphene or reduced graphene oxide can also be combined with other magnetic or non-magnetic materials for broadband Dallenbach absorber design. The high permeability and/or permittivity of the synthesized composites can help to keep the thickness of resulting microwave Dallenbach absorbers within a few millimeters. However, since most of the theoretical investigations of graphene Dallenbach absorbers are based on the measured complex permeability and/or permittivity, further experimental investigations are requested to validate the theoretical results and the effects of incident angles are also to be explored. In addition, while the theoretical explorations on graphene metasurface absorber demonstrate promising reconfigurability, a limited number of experimental investigations only demonstrate mechanically rather than electrically tunable absorption performance due to the limitation of immature fabrication processes. The future research directions of graphene metasurface absorbers include the developments of new design technologies to relax the requirements of device fabrication and new manufacturing technologies to reduce the device cost. The former direction tends to reduce the possibility of device failure caused by the immature fabrication process and the latter direction aims to make graphene metasurface absorbers financially viable for industrial

and military applications. Moreover, graphene may also be combined with other tunable materials such as liquid crystal to realize reconfigurable multi-functional metasurfaces. With the development of graphene synthesis and device fabrication technologies, the graphene metasurface absorbers with reconfigurable absorption performance may play an important role in the development of smart EM wave absorbing materials.

Author Contributions: J.T. participated in resource harvesting as well as writing, editing and reviewing of the whole article. H.S. participated in the writing and reviewing of Section 3. H.H. and Y.B. participated in resource harvesting and the writing of Sections 1 and 2. B.C. and P.T. participated in the resource harvesting and writing of Sections 2 and 3.

Funding: This work is financially supported by the Science and Technology Committee of the Central Military Commission of China on the project “Design and Implementation of Controllable Artificial Electromagnetic Material”.

Acknowledgments: The authors would like to thank Liang Yang from Queen Mary University of London for his continuous support and constructive suggestions.

Conflicts of Interest: The authors declare no conflict of interest.

References

- Novoselov, K.S.; Geim, A.K.; Morozov, S.V.; Jiang, D.; Zhang, Y.; Dubonos, S.V.; Grigorieva, I.V.; Firsov, A.A. Electric field effect in atomically thin carbon films. *Science* **2004**, *306*, 666–669. [[CrossRef](#)] [[PubMed](#)]
- Kubota, Y.; Watanabe, K.; Tsuda, O.; Taniguchi, T. Deep ultraviolet light-emitting hexagonal boron nitride synthesized at atmospheric pressure. *Science* **2007**, *317*, 932–934. [[CrossRef](#)]
- Vogt, P.; De Padova, P.; Quaresima, C.; Avila, J.; Frantzeskakis, E.; Asensio, M.C.; Resta, A.; Ealet, B.; Le Lay, G. Silicene: Compelling experimental evidence for graphenelike two-dimensional silicon. *Phys. Rev. Lett.* **2012**, *108*, 155501. [[CrossRef](#)] [[PubMed](#)]
- Castro, E.V.; Ochoa, H.; Katsnelson, M.; Gorbachev, R.; Elias, D.; Novoselov, K.; Geim, A.; Guinea, F. Limits on charge carrier mobility in suspended graphene due to flexural phonons. *Phys. Rev. Lett.* **2010**, *105*, 266601. [[CrossRef](#)] [[PubMed](#)]
- Tamagnone, M.; Gomez-Diaz, J.; Mosig, J.R.; Perruisseau-Carrier, J. Reconfigurable terahertz plasmonic antenna concept using a graphene stack. *Appl. Phys. Lett.* **2012**, *101*, 214102. [[CrossRef](#)]
- Wang, X.C.; Zhao, W.S.; Hu, J.; Yin, W.Y. Reconfigurable terahertz leaky-wave antenna using graphene-based high-impedance surface. *IEEE Trans. Nanotechnol.* **2015**, *14*, 62–69. [[CrossRef](#)]
- Poumirol, J.M.; Liu, P.Q.; Slipchenko, T.M.; Nikitin, A.Y.; Martin-Moreno, L.; Faist, J.; Kuzmenko, A.B. Electrically controlled terahertz magneto-optical phenomena in continuous and patterned graphene. *Nat. Commun.* **2017**, *8*, 14626. [[CrossRef](#)]
- Hanson, G.W. Dyadic Green’s functions and guided surface waves for a surface conductivity model of graphene. *J. Appl. Phys.* **2008**, *103*, 064302. [[CrossRef](#)]
- Koester, S.J.; Li, H.; Li, M. Switching energy limits of waveguide-coupled graphene-on-graphene optical modulators. *Opt. Express* **2012**, *20*, 20330–20341. [[CrossRef](#)]
- Gosciniak, J.; Tan, D.T. Graphene-based waveguide integrated dielectric-loaded plasmonic electro-absorption modulators. *Nanotechnology* **2013**, *24*, 185202. [[CrossRef](#)]
- Mohsin, M.; Schall, D.; Otto, M.; Nocolak, A.; Neumaier, D.; Kurz, H. Graphene based low insertion loss electro-absorption modulator on SOI waveguide. *Opt. Express* **2014**, *22*, 15292–15297. [[CrossRef](#)] [[PubMed](#)]
- Carrasco, E.; Tamagnone, M.; Mosig, J.R.; Low, T.; Perruisseau-Carrier, J. Gate-controlled mid-infrared light bending with aperiodic graphene nanoribbons array. *Nanotechnology* **2015**, *26*, 134002. [[CrossRef](#)] [[PubMed](#)]
- Giddens, H.; Yang, L.; Tian, J.; Hao, Y. Mid-Infrared Reflect-Array Antenna with Beam Switching Enabled by Continuous Graphene Layer. *IEEE Photonics Technol. Lett.* **2018**, *30*, 748–751. [[CrossRef](#)]
- Wang, C.; Han, X.; Xu, P.; Zhang, X.; Du, Y.; Hu, S.; Wang, J.; Wang, X. The electromagnetic property of chemically reduced graphene oxide and its application as microwave absorbing material. *Appl. Phys. Lett.* **2011**, *98*, 072906. [[CrossRef](#)]
- Song, W.L.; Cao, M.S.; Lu, M.M.; Liu, J.; Yuan, J.; Fan, L.Z. Improved dielectric properties and highly efficient and broadened bandwidth electromagnetic attenuation of thickness-decreased carbon nanosheet/wax composites. *J. Mater. Chem. C* **2013**, *1*, 1846–1854. [[CrossRef](#)]

16. Ren, Y.; Zhu, C.; Qi, L.; Gao, H.; Chen, Y. Growth of γ -Fe₂O₃ nanosheet arrays on graphene for electromagnetic absorption applications. *RSC Adv.* **2014**, *4*, 21510–21516. [[CrossRef](#)]
17. Kang, Y.; Jiang, Z.; Ma, T.; Chu, Z.; Li, G. Hybrids of reduced graphene oxide and hexagonal boron nitride: Lightweight absorbers with tunable and highly efficient microwave attenuation properties. *ACS Appl. Mater. Interfaces* **2016**, *8*, 32468–32476. [[CrossRef](#)]
18. Han, M.; Yin, X.; Hou, Z.; Song, C.; Li, X.; Zhang, L.; Cheng, L. Flexible and thermostable graphene/SiC nanowire foam composites with tunable electromagnetic wave absorption properties. *ACS Appl. Mater. Interfaces* **2017**, *9*, 11803–11810. [[CrossRef](#)]
19. Zhao, H.; Han, X.; Li, Z.; Liu, D.; Wang, Y.; Wang, Y.; Zhou, W.; Du, Y. Reduced graphene oxide decorated with carbon nanopolyhedrons as an efficient and lightweight microwave absorber. *J. Colloid Interface Sci.* **2018**, *528*, 174–183. [[CrossRef](#)]
20. Vasić, B.; Gajić, R. Graphene induced spectral tuning of metamaterial absorbers at mid-infrared frequencies. *Appl. Phys. Lett.* **2013**, *103*, 261111. [[CrossRef](#)]
21. Ye, C.; Zhu, Z.; Xu, W.; Yuan, X.; Qin, S. Electrically tunable absorber based on nonstructured graphene. *J. Opt.* **2015**, *17*, 125009. [[CrossRef](#)]
22. Chen, M.; Sun, W.; Cai, J.; Chang, L.; Xiao, X. Frequency-tunable terahertz absorbers based on graphene metasurface. *Opt. Commun.* **2017**, *382*, 144–150. [[CrossRef](#)]
23. Wang, L.; Ge, S.; Hu, W.; Nakajima, M.; Lu, Y. Graphene-assisted high-efficiency liquid crystal tunable terahertz metamaterial absorber. *Opt. Express* **2017**, *25*, 23873–23879. [[CrossRef](#)] [[PubMed](#)]
24. Yang, L.; Wang, J.; Lu, C. Sensitive perfect absorber with monolayer graphene-based multi-layer dielectric grating structure. *Opt.-Int. J. Light Electron Opt.* **2018**, *158*, 508–513. [[CrossRef](#)]
25. Huang, H.; Xia, H.; Guo, Z.; Zeng, J.; Li, H.; Xie, D. Temperature-insensitive and separately tunable dual-band metamaterial absorber based on graphene at mid-infrared regions. *Results Phys.* **2018**, *10*, 1015–1021. [[CrossRef](#)]
26. Zhang, J.; Tian, J.; Li, L. A dual-band tunable metamaterial near-unity absorber composed of periodic cross and disk graphene arrays. *IEEE Photonics J.* **2018**, *10*, 1–12. [[CrossRef](#)]
27. Liu, C.; Qi, L.; Zhang, X. Broadband graphene-based metamaterial absorbers. *AIP Adv.* **2018**, *8*, 015301. [[CrossRef](#)]
28. Sun, P.; You, C.; Mahigir, A.; Liu, T.; Xia, F.; Kong, W.; Veronis, G.; Dowling, J.P.; Dong, L.; Yun, M. Graphene-based dual-band independently tunable infrared absorber. *Nanoscale* **2018**, *10*, 15564–15570. [[CrossRef](#)]
29. He, G.; Stiens, J. Enhanced Terahertz Absorption of Graphene Composite Integrated with Double Circular Metal Ring Array. *Plasmonics* **2018**, *13*, 1705–1710. [[CrossRef](#)]
30. Luo, X.; Liu, Z.; Wang, L.; Liu, J.; Lin, Q. Tunable ultra-narrowband and wide-angle graphene-based perfect absorber in the optical communication region. *Appl. Phys. Express* **2018**, *11*, 105102. [[CrossRef](#)]
31. Mou, N.; Sun, S.; Dong, H.; Dong, S.; He, Q.; Zhou, L.; Zhang, L. Hybridization-induced broadband terahertz wave absorption with graphene metasurfaces. *Opt. Express* **2018**, *26*, 11728–11736. [[CrossRef](#)] [[PubMed](#)]
32. Salisbury, W.W. Absorbent Body for Electromagnetic Waves. U.S. Patent 2,599,944, 1952.
33. Du Toit, L.J. The design of Jauman absorbers. *IEEE Antennas Propag. Mag.* **1994**, *36*, 17–25. [[CrossRef](#)]
34. Dällenbach, W.; Kleinsteuber, W. Reflection and absorption of decimeter-waves by plane dielectric layers. *Hochfreq. u. Elektroak* **1938**, *51*, 152–156.
35. Wu, B.; Tuncer, H.M.; Naeem, M.; Yang, B.; Cole, M.T.; Milne, W.I.; Hao, Y. Experimental demonstration of a transparent graphene millimetre wave absorber with 28% fractional bandwidth at 140 GHz. *Sci. Rep.* **2014**, *4*, 4130. [[CrossRef](#)]
36. Liu, J.T.; Liu, N.H.; Wang, L.; Deng, X.H.; Su, F.H. Gate-tunable nearly total absorption in graphene with resonant metal back reflector. *EPL (Europhys. Lett.)* **2013**, *104*, 57002. [[CrossRef](#)]
37. Xu, B.z.; Gu, C.q.; Li, Z.; Niu, Z. A novel structure for tunable terahertz absorber based on graphene. *Opt. Express* **2013**, *21*, 23803–23811. [[CrossRef](#)]
38. Min Woo, J.; Kim, M.S.; Woong Kim, H.; Jang, J.H. Graphene based salisbury screen for terahertz absorber. *Appl. Phys. Lett.* **2014**, *104*, 081106. [[CrossRef](#)]
39. Balci, O.; Polat, E.O.; Kakenov, N.; Kocabas, C. Graphene-enabled electrically switchable radar-absorbing surfaces. *Nat. Commun.* **2015**, *6*, 6628. [[CrossRef](#)] [[PubMed](#)]

40. Kakenov, N.; Balci, O.; Takan, T.; Ozkan, V.A.; Altan, H.; Kocabas, C. Observation of gate-tunable coherent perfect absorption of terahertz radiation in graphene. *ACS Photonics* **2016**, *3*, 1531–1535. [[CrossRef](#)]
41. Thareja, V.; Kang, J.H.; Yuan, H.; Milaninia, K.M.; Hwang, H.Y.; Cui, Y.; Kik, P.G.; Brongersma, M.L. Electrically tunable coherent optical absorption in graphene with ion gel. *Nano Lett.* **2015**, *15*, 1570–1576. [[CrossRef](#)]
42. Ying, X.; Pu, Y.; Li, Z.; Liu, Z.; Jiang, Y. Absorption enhancement of graphene Salisbury screen in the mid-infrared regime. *J. Opt.* **2015**, *44*, 59–67. [[CrossRef](#)]
43. Ma, Z.; Zhang, Y.; Cao, C.; Yuan, J.; Liu, Q.; Wang, J. Attractive microwave absorption and the impedance match effect in zinc oxide and carbonyl iron composite. *Phys. B Condens. Matter* **2011**, *406*, 4620–4624. [[CrossRef](#)]
44. Bai, X.; Zhai, Y.; Zhang, Y. Green approach to prepare graphene-based composites with high microwave absorption capacity. *J. Phys. Chem. C* **2011**, *115*, 11673–11677. [[CrossRef](#)]
45. Singh, V.K.; Shukla, A.; Patra, M.K.; Saini, L.; Jani, R.K.; Vadera, S.R.; Kumar, N. Microwave absorbing properties of a thermally reduced graphene oxide/nitrile butadiene rubber composite. *Carbon* **2012**, *50*, 2202–2208. [[CrossRef](#)]
46. Liu, P.B.; Huang, Y.; Sun, X. Excellent electromagnetic absorption properties of poly (3,4-ethylenedioxythiophene)-reduced graphene oxide–Co₃O₄ composites prepared by a hydrothermal method. *ACS Appl. Mater. Interfaces* **2013**, *5*, 12355–12360. [[CrossRef](#)] [[PubMed](#)]
47. Ameer, S.; Gul, I.H. Influence of Reduced Graphene Oxide on Effective Absorption Bandwidth Shift of Hybrid Absorbers. *PLoS ONE* **2016**, *11*, e0153544. [[CrossRef](#)] [[PubMed](#)]
48. Zhang, Y.; Huang, Y.; Zhang, T.; Chang, H.; Xiao, P.; Chen, H.; Huang, Z.; Chen, Y. Broadband and tunable high-performance microwave absorption of an ultralight and highly compressible graphene foam. *Adv. Mater.* **2015**, *27*, 2049–2053. [[CrossRef](#)] [[PubMed](#)]
49. Han, M.; Yin, X.; Duan, W.; Ren, S.; Zhang, L.; Cheng, L. Hierarchical graphene/SiC nanowire networks in polymer-derived ceramics with enhanced electromagnetic wave absorbing capability. *J. Eur. Ceram. Soc.* **2016**, *36*, 2695–2703. [[CrossRef](#)]
50. Liu, P.; Ng, V.M.H.; Yao, Z.; Zhou, J.; Lei, Y.; Yang, Z.; Kong, L.B. Microwave absorption properties of double-layer absorbers based on Co_{0.2}Ni_{0.4}Zn_{0.4}Fe₂O₄ ferrite and reduced graphene oxide composites. *J. Alloys Compd.* **2017**, *701*, 841–849. [[CrossRef](#)]
51. Li, J.; Zhang, D.; Qi, H.; Wang, G.; Tang, J.; Tian, G.; Liu, A.; Yue, H.; Yu, Y.; Feng, S. Economical synthesis of composites of FeNi alloy nanoparticles evenly dispersed in two-dimensional reduced graphene oxide as thin and effective electromagnetic wave absorbers. *RSC Adv.* **2018**, *8*, 8393–8401. [[CrossRef](#)]
52. Shu, R.; Zhang, G.; Zhang, J.; Wang, X.; Wang, M.; Gan, Y.; Shi, J.; He, J. Fabrication of reduced graphene oxide/multi-walled carbon nanotubes/zinc ferrite hybrid composites as high-performance microwave absorbers. *J. Alloys Compd.* **2018**, *736*, 1–11. [[CrossRef](#)]
53. Quan, B.; Liang, X.; Ji, G.; Lv, J.; Dai, S.; Xu, G.; Du, Y. Laminated graphene oxide-supported high-efficiency microwave absorber fabricated by an *insitu* growth approach. *Carbon* **2018**, *129*, 310–320. [[CrossRef](#)]
54. Zhang, N.; Huang, Y.; Liu, P.; Ding, X.; Zong, M.; Wang, M. Synthesis of magnetical nanoparticles decorated with reduced graphene oxide as an efficient broad band EM wave absorber. *J. Alloys Compd.* **2017**, *692*, 639–646. [[CrossRef](#)]
55. Li, J.; Wang, L.; Zhang, D.; Qu, Y.; Wang, G.; Tian, G.; Liu, A.; Yue, H.; Feng, S. Reduced graphene oxide modified mesoporous FeNi alloy/carbon microspheres for enhanced broadband electromagnetic wave absorbers. *Mater. Chem. Front.* **2017**, *1*, 1786–1794. [[CrossRef](#)]
56. Song, C.; Yin, X.; Han, M.; Li, X.; Hou, Z.; Zhang, L.; Cheng, L. Three-dimensional reduced graphene oxide foam modified with ZnO nanowires for enhanced microwave absorption properties. *Carbon* **2017**, *116*, 50–58. [[CrossRef](#)]
57. Wang, L.; Xing, H.; Gao, S.; Ji, X.; Shen, Z. Porous flower-like NiO@ graphene composites with superior microwave absorption properties. *J. Mater. Chem. C* **2017**, *5*, 2005–2014. [[CrossRef](#)]
58. Liu, P.; Huang, Y.; Yan, J.; Zhao, Y. Magnetic graphene@ PANI@ porous TiO₂ ternary composites for high-performance electromagnetic wave absorption. *J. Mater. Chem. C* **2016**, *4*, 6362–6370. [[CrossRef](#)]
59. Qu, B.; Zhu, C.; Li, C.; Zhang, X.; Chen, Y. Coupling hollow Fe₃O₄-Fe nanoparticles with graphene sheets for high-performance electromagnetic wave absorbing material. *ACS Appl. Mater. Interfaces* **2016**, *8*, 3730–3735. [[CrossRef](#)]

60. Ren, F.; Zhu, G.; Ren, P.; Wang, K.; Cui, X.; Yan, X. Cyanate ester resin filled with graphene nanosheets and CoFe_2O_4 -reduced graphene oxide nanohybrids as a microwave absorber. *Appl. Surf. Sci.* **2015**, *351*, 40–47. [[CrossRef](#)]
61. Wang, J.; Sun, Y.; Chen, W.; Wang, T.; Xu, R.; Wang, J. Enhanced microwave absorption performance of lightweight absorber based on reduced graphene oxide and Ag-coated hollow glass spheres/epoxy composite. *J. Appl. Phys.* **2015**, *117*, 154903. [[CrossRef](#)]
62. Sun, C.; Jiang, W.; Wang, Y.; Sun, D.; Liu, J.; Li, P.; Li, F. Magnetic and electromagnetic absorption properties of FeNi alloy nanoparticles supported by reduced graphene oxide. *Phys. Status Solidi (RRL)–Rapid Res. Lett.* **2014**, *8*, 141–145. [[CrossRef](#)]
63. Wang, L.; Huang, Y.; Sun, X.; Huang, H.; Liu, P.; Zong, M.; Wang, Y. Synthesis and microwave absorption enhancement of graphene@ Fe_3O_4 @ SiO_2 @NiO nanosheet hierarchical structures. *Nanoscale* **2014**, *6*, 3157–3164. [[CrossRef](#)] [[PubMed](#)]
64. Wu, F.; Xia, Y.; Wang, Y.; Wang, M. Two-step reduction of self-assembled three-dimensional (3D) reduced graphene oxide (RGO)/zinc oxide (ZnO) nanocomposites for electromagnetic absorption. *J. Mater. Chem. A* **2014**, *2*, 20307–20315. [[CrossRef](#)]
65. Zhao, X.; Zhang, Z.; Wang, L.; Xi, K.; Cao, Q.; Wang, D.; Yang, Y.; Du, Y. Excellent microwave absorption property of graphene-coated Fe nanocomposites. *Sci. Rep.* **2013**, *3*, 3421. [[CrossRef](#)] [[PubMed](#)]
66. Zhang, X.J.; Wang, G.S.; Wei, Y.Z.; Guo, L.; Cao, M.S. Polymer-composite with high dielectric constant and enhanced absorption properties based on graphene–CuS nanocomposites and polyvinylidene fluoride. *J. Mater. Chem. A* **2013**, *1*, 12115–12122. [[CrossRef](#)]
67. Sun, X.; He, J.; Li, G.; Tang, J.; Wang, T.; Guo, Y.; Xue, H. Laminated magnetic graphene with enhanced electromagnetic wave absorption properties. *J. Mater. Chem. C* **2013**, *1*, 765–777. [[CrossRef](#)]
68. Liu, P.; Huang, Y.; Wang, L.; Zhang, W. Synthesis and excellent electromagnetic absorption properties of polypyrrole-reduced graphene oxide– Co_3O_4 nanocomposites. *J. Alloys Compd.* **2013**, *573*, 151–156. [[CrossRef](#)]
69. Wang, T.; Liu, Z.; Lu, M.; Wen, B.; Ouyang, Q.; Chen, Y.; Zhu, C.; Gao, P.; Li, C.; Cao, M.; others. Graphene– Fe_3O_4 nanohybrids: Synthesis and excellent electromagnetic absorption properties. *J. Appl. Phys.* **2013**, *113*, 024314. [[CrossRef](#)]
70. Yu, H.; Wang, T.; Wen, B.; Lu, M.; Xu, Z.; Zhu, C.; Chen, Y.; Xue, X.; Sun, C.; Cao, M. Graphene/polyaniline nanorod arrays: Synthesis and excellent electromagnetic absorption properties. *J. Mater. Chem.* **2012**, *22*, 21679–21685. [[CrossRef](#)]
71. Xu, H.L.; Bi, H.; Yang, R.B. Enhanced microwave absorption property of bowl-like Fe_3O_4 hollow spheres/reduced graphene oxide composites. *J. Appl. Phys.* **2012**, *111*, 07A522. [[CrossRef](#)]
72. Grande, M.; Vincenti, M.; Stomeo, T.; De Ceglia, D.; Petruzzelli, V.; De Vittorio, M.; Scalora, M.; D’Orazio, A. Absorption and losses in one-dimensional photonic-crystal-based absorbers incorporating graphene. *IEEE Photonics J.* **2014**, *6*, 1–8. [[CrossRef](#)]
73. Ning, R.; Liu, S.; Zhang, H.; Bian, B.; Kong, X. A wide-angle broadband absorber in graphene-based hyperbolic metamaterials. *Eur. Phys. J.-Appl. Phys.* **2014**, *68*. [[CrossRef](#)]
74. Wang, X.; Jiang, X.; You, Q.; Guo, J.; Dai, X.; Xiang, Y. Tunable and multichannel terahertz perfect absorber due to Tamm surface plasmons with graphene. *Photonics Res.* **2017**, *5*, 536–542. [[CrossRef](#)]
75. Kong, X.k.; Shi, X.z.; Mo, J.j.; Fang, Y.t.; Chen, X.l.; Liu, S.b. Tunable multichannel absorber composed of graphene and doped periodic structures. *Opt. Commun.* **2017**, *383*, 391–396. [[CrossRef](#)]
76. Madani, A.; Babaei, M. Tunable polarization sensitive absorber made of graphene-based hyperbolic metamaterials. *Superlattices Microstruct.* **2017**, *102*, 470–476. [[CrossRef](#)]
77. Zou, X.; Zheng, G.; Chen, Y.; Xu, L.; Lai, M. Multiple resonant absorber with prism-incorporated graphene and one-dimensional photonic crystals in the visible and near-infrared spectral range. *Superlattices Microstruct.* **2018**, *116*, 88–94. [[CrossRef](#)]
78. Alaei, R.; Farhat, M.; Rockstuhl, C.; Lederer, F. A perfect absorber made of a graphene micro-ribbon metamaterial. *Opt. Express* **2012**, *20*, 28017–28024. [[CrossRef](#)]
79. Li, X.; Yi, H.; Zhang, J.; Feng, J.; Li, F.; Xue, D.; Zhang, H.; Peng, Y.; Mellors, N.J. Fe_3O_4 –graphene hybrids: Nanoscale characterization and their enhanced electromagnetic wave absorption in gigahertz range. *J. Nanopart. Res.* **2013**, *15*, 1472. [[CrossRef](#)]
80. Hong, S.K.; Kim, K.Y.; Kim, T.Y.; Kim, J.H.; Park, S.W.; Kim, J.H.; Cho, B.J. Electromagnetic interference shielding effectiveness of monolayer graphene. *Nanotechnology* **2012**, *23*, 455704. [[CrossRef](#)]

81. Wan, Y.J.; Zhu, P.L.; Yu, S.H.; Sun, R.; Wong, C.P.; Liao, W.H. Ultralight, super-elastic and volume-preserving cellulose fiber/graphene aerogel for high-performance electromagnetic interference shielding. *Carbon* **2017**, *115*, 629–639. [[CrossRef](#)]
82. Liu, Y.; Zeng, J.; Han, D.; Wu, K.; Yu, B.; Chai, S.; Chen, F.; Fu, Q. Graphene enhanced flexible expanded graphite film with high electric, thermal conductivities and EMI shielding at low content. *Carbon* **2018**, *133*, 435–445. [[CrossRef](#)]
83. Grande, M.; Vincenti, M.; Stomeo, T.; Bianco, G.; De Ceglia, D.; Aközbeek, N.; Petruzzelli, V.; Bruno, G.; De Vittorio, M.; Scalora, M.; others. Graphene-based absorber exploiting guided mode resonances in one-dimensional gratings. *Opt. Express* **2014**, *22*, 31511–31519. [[CrossRef](#)] [[PubMed](#)]
84. Long, Y.; Li, Y.; Shen, L.; Liang, W.; Deng, H.; Xu, H. Dually guided-mode-resonant graphene perfect absorbers with narrow bandwidth for sensors. *J. Phys. D Appl. Phys.* **2016**, *49*, 32LT01. [[CrossRef](#)]
85. Zhang, H.J.; Zheng, G.G.; Chen, Y.Y.; Zou, X.J.; Xu, L.H. A Perfect Graphene Absorber with Waveguide Coupled High-Contrast Gratings. *Chin. Phys. Lett.* **2018**, *35*, 038102. [[CrossRef](#)]
86. Nefedov, I.S.; Valagiannopoulos, C.A.; Melnikov, L.A. Perfect absorption in graphene multilayers. *J. Opt.* **2013**, *15*, 114003. [[CrossRef](#)]
87. Chen, P.Y.; Farhat, M.; Bağcı, H. Graphene metascreen for designing compact infrared absorbers with enhanced bandwidth. *Nanotechnology* **2015**, *26*, 164002. [[CrossRef](#)] [[PubMed](#)]
88. Thongrattanasiri, S.; Koppens, F.H.; De Abajo, F.J.G. Complete optical absorption in periodically patterned graphene. *Phys. Rev. Lett.* **2012**, *108*, 047401. [[CrossRef](#)]
89. Cai, Y.; Zhu, J.; Liu, Q.H.; Lin, T.; Zhou, J.; Ye, L.; Cai, Z. Enhanced spatial near-infrared modulation of graphene-loaded perfect absorbers using plasmonic nanoslits. *Opt. Express* **2015**, *23*, 32318–32328. [[CrossRef](#)]
90. Meng, H.; Wang, L.; Liu, G.; Xue, X.; Lin, Q.; Zhai, X. Tunable graphene-based plasmonic multispectral and narrowband perfect metamaterial absorbers at the mid-infrared region. *Applied Optics* **2017**, *56*, 6022–6027. [[CrossRef](#)]
91. Xu, H.; Xiong, C.; Chen, Z.; Zheng, M.; Zhao, M.; Zhang, B.; Li, H. Dynamic plasmon-induced transparency modulator and excellent absorber-based terahertz planar graphene metamaterial. *JOSA B* **2018**, *35*, 1463–1468. [[CrossRef](#)]
92. Chen, Y.; Zhang, A.; Ding, L.; Liu, Y.; Lu, H. A three-dimensional absorber hybrid with polar oxygen functional groups of MWNs/graphene with enhanced microwave absorbing properties. *Compos. Part B Eng.* **2017**, *108*, 386–392. [[CrossRef](#)]
93. Hashemi, M.; Farzad, M.H.; Mortensen, N.A.; Xiao, S. Enhanced absorption of graphene in the visible region by use of plasmonic nanostructures. *J. Opt.* **2013**, *15*, 055003. [[CrossRef](#)]
94. Song, S.; Chen, Q.; Jin, L.; Sun, F. Great light absorption enhancement in a graphene photodetector integrated with a metamaterial perfect absorber. *Nanoscale* **2013**, *5*, 9615–9619. [[CrossRef](#)]
95. Zhang, Y.; Shi, Y.; Liang, C.H. Broadband tunable graphene-based metamaterial absorber. *Opt. Mater. Express* **2016**, *6*, 3036–3044. [[CrossRef](#)]
96. Jia, X.; Wang, X.; Yuan, C.; Meng, Q.; Zhou, Z. Novel dynamic tuning of broadband visible metamaterial perfect absorber using graphene. *J. Appl. Phys.* **2016**, *120*, 033101. [[CrossRef](#)]
97. Zare, M.S.; Nozhat, N.; Rashiditabar, R. Tunable graphene based plasmonic absorber with grooved metal film in near infrared region. *Opt. Commun.* **2017**, *398*, 56–61. [[CrossRef](#)]
98. Lee, S.; Tran, T.Q.; Heo, H.; Kim, M.; Kim, S. A proposal of a perfect graphene absorber with enhanced design and fabrication tolerance. *Sci. Rep.* **2017**, *7*, 4760. [[CrossRef](#)]
99. Liao, Y.L.; Zhao, Y. Graphene-based tunable ultra-narrowband mid-infrared TE-polarization absorber. *Opt. Express* **2017**, *25*, 32080–32089. [[CrossRef](#)]
100. Fan, Y.; Guo, C.; Zhu, Z.; Xu, W.; Wu, F.; Yuan, X.; Qin, S. Monolayer-graphene-based broadband and wide-angle perfect absorption structures in the near infrared. *Sci. Rep.* **2018**, *8*, 13709. [[CrossRef](#)]
101. He, X.; Zhong, X.; Lin, F.; Shi, W. Investigation of graphene assisted tunable terahertz metamaterials absorber. *Opt. Mater. Express* **2016**, *6*, 331–342. [[CrossRef](#)]
102. Yao, G.; Ling, F.; Yue, J.; Luo, C.; Luo, Q.; Yao, J. Dynamically electrically tunable broadband absorber based on graphene analog of electromagnetically induced transparency. *IEEE Photonics J.* **2016**, *8*, 1–8. [[CrossRef](#)]
103. Arik, K.; AbdollahRamezani, S.; Khavasi, A. Polarization insensitive and broadband terahertz absorber using graphene disks. *Plasmonics* **2017**, *12*, 393–398. [[CrossRef](#)]

104. Zhou, Q.; Liu, P.; Bian, L.a.; Liu, H.; Liu, C.; Chen, G. Controlling enhanced absorption in graphene metamaterial. *Opt. Commun.* **2018**, *413*, 310–316. [[CrossRef](#)]
105. Xu, B.; Gu, C.; Li, Z.; Liu, L.; Niu, Z. A novel absorber with tunable bandwidth based on graphene. *IEEE Antennas Wirel. Propag. Lett.* **2014**, *13*, 822–825.
106. Zhang, Y.; Feng, Y.; Zhu, B.; Zhao, J.; Jiang, T. Graphene based tunable metamaterial absorber and polarization modulation in terahertz frequency. *Opt. Express* **2014**, *22*, 22743–22752. [[CrossRef](#)]
107. Yu-Ping, Z.; Tong-Tong, L.; Huan-Huan, L.; Xiao-Yan, H.; Xiao, Z.; Shi-Lin, X.; Hui-Yun, Z. Graphene-based tunable polarization insensitive dual-band metamaterial absorber at mid-infrared frequencies. *Chin. Phys. Lett.* **2015**, *32*, 068101. [[CrossRef](#)]
108. Yao, G.; Ling, F.; Yue, J.; Luo, C.; Ji, J.; Yao, J. Dual-band tunable perfect metamaterial absorber in the THz range. *Opt. Express* **2016**, *24*, 1518–1527. [[CrossRef](#)]
109. Wang, F.; Huang, S.; Li, L.; Chen, W.; Xie, Z. Dual-band tunable perfect metamaterial absorber based on graphene. *Appl. Opt.* **2018**, *57*, 6916–6922. [[CrossRef](#)] [[PubMed](#)]
110. Parvaz, R.; Karami, H. Far-infrared multi-resonant graphene-based metamaterial absorber. *Opt. Commun.* **2017**, *396*, 267–274. [[CrossRef](#)]
111. Zhang, Y.; Li, Y.; Cao, Y.; Liu, Y.; Zhang, H. Graphene induced tunable and polarization-insensitive broadband metamaterial absorber. *Opt. Commun.* **2017**, *382*, 281–287. [[CrossRef](#)]
112. Zhihong, Z.; Chucai, G.; Jianfa, Z.; Ken, L.; Xiaodong, Y.; Shiqiao, Q. Broadband single-layered graphene absorber using periodic arrays of graphene ribbons with gradient width. *Appl. Phys. Express* **2014**, *8*, 015102. [[CrossRef](#)]
113. Ye, L.; Chen, Y.; Cai, G.; Liu, N.; Zhu, J.; Song, Z.; Liu, Q.H. Broadband absorber with periodically sinusoidally-patterned graphene layer in terahertz range. *Opt. Express* **2017**, *25*, 11223–11232. [[CrossRef](#)] [[PubMed](#)]
114. Ye, L.; Chen, X.; Zhuo, J.; Han, F.; Liu, Q.H. Actively tunable broadband terahertz absorption using periodically square-patterned graphene. *Appl. Phys. Express* **2018**, *11*, 102201. [[CrossRef](#)]
115. Agarwal, S.; Prajapati, Y. Broadband and polarization-insensitive helix metamaterial absorber using graphene for terahertz region. *Appl. Phys. A* **2016**, *122*, 561. [[CrossRef](#)]
116. Amin, M.; Farhat, M.; Bağcı, H. An ultra-broadband multilayered graphene absorber. *Opt. Express* **2013**, *21*, 29938–29948. [[CrossRef](#)]
117. Wang, Y.; Song, M.; Pu, M.; Gu, Y.; Hu, C.; Zhao, Z.; Wang, C.; Yu, H.; Luo, X. Staked Graphene for Tunable Terahertz Absorber with Customized Bandwidth. *Plasmonics* **2016**, *11*, 1201–1206. [[CrossRef](#)]
118. Xiao, B.; Gu, M.; Xiao, S. Broadband, wide-angle and tunable terahertz absorber based on cross-shaped graphene arrays. *Appl. Opt.* **2017**, *56*, 5458–5462. [[CrossRef](#)] [[PubMed](#)]
119. Zhang, Y.C.; Fang, Y.T.; Cai, Q. Broad band absorber based on cascaded metamaterial layers including graphene. *Waves Random Complex Media* **2017**, *28*, 287–299. [[CrossRef](#)]
120. Fardoost, A.; Vanani, F.G.; Safian, R.; others. Design of a multilayer graphene-based ultrawideband terahertz absorber. *IEEE Trans. Nanotechnol.* **2017**, *16*, 68–74.
121. Wang, J.; Gao, C.N.; Jiang, Y.N.; Akwuruoha, C.N. Ultra-broadband and polarization-independent planar absorber based on multilayered graphene. *Chin. Phys. B* **2017**, *26*, 114102. [[CrossRef](#)]
122. Huang, X.; Pan, K.; Hu, Z. Experimental demonstration of printed graphene nano-flakes enabled flexible and conformable wideband radar absorbers. *Sci. Rep.* **2016**, *6*, 38197. [[CrossRef](#)] [[PubMed](#)]
123. Ye, F.; Song, C.; Zhou, Q.; Yin, X.; Han, M.; Li, X.; Zhang, L.; Cheng, L. Broadband Microwave Absorbing Composites with a Multi-Scale Layered Structure Based on Reduced Graphene Oxide Film as the Frequency Selective Surface. *Materials* **2018**, *11*, 1771. [[CrossRef](#)] [[PubMed](#)]
124. Wang, Z.; Zhou, M.; Lin, X.; Liu, H.; Wang, H.; Yu, F.; Lin, S.; Li, E.; Chen, H. A circuit method to integrate metamaterial and graphene in absorber design. *Opt. Commun.* **2014**, *329*, 76–80. [[CrossRef](#)]
125. Zhang, L.; Hu, F.; Xu, X.; Wang, Y.; Guo, E. Design of separately tunable terahertz two-peak absorber based on graphene. *Opt. Commun.* **2016**, *369*, 65–71. [[CrossRef](#)]
126. Li, L.; Cao, M.; Li, T.; Meng, L.; Zhang, H.; Zhang, Y. Complementary graphene metamaterial with independently tunable dual absorption bands at terahertz frequency. *Mater. Res. Express* **2017**, *4*, 105801. [[CrossRef](#)]

127. Zhang, Y.; Li, T.; Chen, Q.; Zhang, H.; O'Hara, J.F.; Abele, E.; Taylor, A.J.; Chen, H.T.; Azad, A.K. Independently tunable dual-band perfect absorber based on graphene at mid-infrared frequencies. *Sci. Rep.* **2015**, *5*, 18463. [[CrossRef](#)] [[PubMed](#)]
128. Zhao, Y.T.; Wu, B.; Huang, B.J.; Cheng, Q. Switchable broadband terahertz absorber/reflector enabled by hybrid graphene-gold metasurface. *Opt. Express* **2017**, *25*, 7161–7169. [[CrossRef](#)]
129. Ghods, M.M.; Rezaei, P. Ultra-wideband microwave absorber based on uncharged graphene layers. *J. Electromagn. Waves Appl.* **2018**, *32*, 1950–1960. [[CrossRef](#)]
130. Masuminia, S.; Ghobadi, C.; Nourinia, J.; Karamirad, M.; Mohammadi, B. A Novel Tunable Graphene Based Terahertz Absorber with Polarization Insensitive. *Appl. Comput. Electromagn. Soc. J.* **2016**, *31*, 1439–1444.
131. Biabanifard, S.; Biabanifard, M.; Asgari, S.; Asadi, S.; Mustapha, C. Tunable ultra-wideband terahertz absorber based on graphene disks and ribbons. *Opt. Commun.* **2018**, *427*, 418–425. [[CrossRef](#)]
132. Liu, X.; Yuan, W.; Yuan, Y.; Wei, W.; Yuan, N. A Novel Tunable Broadband Absorber based on Graphene. In *IOP Conference Series: Materials Science and Engineering*; IOP Publishing: Bristol, UK, 2018; Volume 382, p. 022071.
133. Yi, D.; Wei, X.C.; Xu, Y.L. Tunable microwave absorber based on patterned graphene. *IEEE Trans. Microw. Theory Techniques* **2017**, *65*, 2819–2826. [[CrossRef](#)]
134. Chen, H.; Lu, W.B.; Liu, Z.G.; Zhang, J.; Zhang, A.Q.; Wu, B. Experimental Demonstration of Microwave Absorber Using Large-Area Multilayer Graphene-Based Frequency Selective Surface. *IEEE Trans. Microw. Theory Tech.* **2018**. [[CrossRef](#)]
135. Jiang, Y.; De Zhang, H.; Wang, J.; Gao, C.N.; Wang, J.; Cao, W.P. Design and performance of a terahertz absorber based on patterned graphene. *Opt. Lett.* **2018**, *43*, 4296–4299. [[CrossRef](#)] [[PubMed](#)]



© 2019 by the authors. Licensee MDPI, Basel, Switzerland. This article is an open access article distributed under the terms and conditions of the Creative Commons Attribution (CC BY) license (<http://creativecommons.org/licenses/by/4.0/>).